# MAGNETIC RESONANCE IMAGING OF CEREBRAL PERFUSION USING DSC AND ASL TECHNIQUES AT 3T

by

**Onur Özyurt**

B.S, Physics, Middle East Technical University, 2005

Submitted to the Institute of Biomedical Engineering
in partial fulfillment of the requirements
for the degree of
Master of Science
in
Biomedical Engineering

Boğaziçi University
Month 2008

# MAGNETIC RESONANCE IMAGING OF CEREBRAL PERFUSION USING DSC AND ASL TECHNIQUES AT 3T

## APPROVED BY:

Assoc. Prof. Dr. Cengizhan Öztürk .....
(Thesis Advisor)

Prof. Dr. Ahmet Ademoğlu .....

Assoc. Prof. Dr. Kubilay Aydın .....

**DATE OF APPROVAL:** 21.01.2008

# ACKNOWLEDGMENTS

I am greatly thankful to my advisor Cengizhan Öztürk for his guidance during the study and critical reviews on the written material of the thesis. His insight about every subject have already opened new roads in my mind.

This work started with the suggestion of Uzay Emir, I want to thank him for encouragement, motivation and technical support that provided me.

This is the first study in Turkey which the baseline cerebral perfusion is measured quantitatively by using a non-invasive technique. I deeply appreciate to Dr. Alp Dinçer for his guidance which made this study possible and for critical reviewing of the experimental results. He provided valuable support on clinical aspects and informed me about the needs of the field.

I am also grateful to Cem Işık, Barış Atakay, Serhat Güney Yılmaz, Ömer Arslan for sharing their technical experience during the scans; Emrah Motugan, Mesut Gökbayrak, Hasan Büktel, Özgür Genç, Alper Yaman, Seda Demirel for their patience and support and Volkan Büyükgüngör for his collaboration.

Lastly, I would like to express special thanks and love to my mother Ülkü Özyurt. She was the source of life (in the beginning), and her moral support was very valuable for me. This study is dedicated to her.

# ABSTRACT

## MAGNETIC RESONANCE IMAGING OF CEREBRAL PERFUSION USING DSC AND ASL TECHNIQUES AT 3T

Magnetic resonance imaging (MRI) of cerebral perfusion is used as a complementary procedure in diagnosis of cerebral lesions. In this work, cerebral perfusion and perfusion related parameters are measured in terms of arterial spin labeling (ASL) and dynamic susceptibility contrast (DSC) techniques using MRI. All scans were performed at 3T in two healthy volunteers and two patients with cerebral lesions.

In DSC, contrast agent concentration- time curves were obtained from the measurements. Then, singular value decomposition (SVD) method with constant threshold is used on the arterial and tissue pixels. As a result, relative quantitative values of cerebral blood flow (CBF), cerebral blood volume (CBV) and mean transit time (MTT) were calculated.

In ASL, both the single and multiple subtraction methods are used in the subjects. Quantitative CBF maps are obtained as a result of both methods; additionally, transit delay of blood was quantified using multiple-subtraction method. For the patient and volunteer scans, perfusion values obtained by ASL were observed to be in good agreement with relative DSC results or with quantitative PET results in literature which are used as the gold standard. Comparisons were based on the mean CBF values in various tissue kinds of brain.

**Keywords:** Brain, MRI, Perfusion, CBF, multiple subtraction, ASL, DSC.

# ÖZET

## BEYİN PERFÜZYONUNUN ASL VE DSC TEKNİKLERİ İLE 3T MANYETİK REZONANS GÖRÜNTÜLENMESİ

Beyin perfüzyonunun manyetik rezonans görüntülenmesi (MRG), beyin lezyonlarının tanısında da kullanılan bir yöntemdir. Bu çalışmada, beyin perfüzyonu ASL ve DSC teknikleri ile ölçülmüştür. Çekimler, 3 Tesla'lık MR kullanılarak iki sağlıklı gönüllüde ve iki beyin lezyonlu hastada yapılmıştır.

DSC tekniğinde, çekim sonuçları kullanılarak, kontrast maddenin zamanla değişimi her doku için ölçüldü. Beyni besleyen atardamarların ve beyin dokularının bu sonuçları, sabit eşikli SVD yönteminde kullanıldı. Sonuçta, bağıl değerli beyinsel kan hacmi (CBV), beyinsel kan akışı (CBF) ve ortalama geçiş süresi (MTT) haritaları elde edildi.

ASL çekimlerinde, tekli ve çoklu ölçüm metodları kullanıldı. Her iki metodla da tam nicel CBF değerleri hesaplanırken çoklu ölçüm metoduyla buna ek olarak kanın iletim gecikmesi de hesaplandı. Hem hasta hem de gönüllülerde ölçülen tam nicel ASL perfüzyon sonuçlarının, bağıl DSC sonuçları ve standart olarak kabul edilen PET'in literatür değerleriyle uyumlu olduğu gözlendi. Bütün karşılaştırmalar beynin özel doku türlerindeki ortalama CBF sonuçları baz alınarak yapıldı.

**Anahtar Sözcükler:** Beyin, MRG, Perfüzyon, ASL, DSC.

# TABLE OF CONTENTS

# LIST OF FIGURES

# LIST OF TABLES

# LIST OF SYMBOLS

| | |
|---|---|
| K | Ratio of blood volume hematocrit to venous hematocrit |
| $\lambda$ | Blood-brain partition coefficient |
| V | Volume |
| q | Volume of injected indicator |
| c(t), $C_v$(t) | Concentration of agent in the vein |
| F | Flow |
| h(t) | Frequency function of traversal times |
| $\bar{t}$ | Mean transit time |
| $\otimes$ | Convolution Operator |
| R(t) | Residue function |
| $C_a$(t) | Concentration of agent in the artery |
| $C_{VOI}$(t) | Concentration of agent in imaged voxel |
| W | Total weight of brain |
| k | Calibration Factor |
| $T_R$ | Repetition time |
| $T_E$ | Echo time |
| $B_0$ | Static magnetic field |
| w | Angular frequency of precession |
| $R_2$ | Transverse relaxivity |
| $T_1$ | Longitudinal relaxation time constant |
| $T_2$ | Transverse relaxation time constant |
| $M_{0B}$ | Equilibrium magnetization of blood |
| $\tau$ | Tag width (or intrinsic duration) |
| $\delta$t, $\Delta$t | Transit time (or transit delay) |
| q | Calibration factor in ASL |
| TI, $\Delta$TI | Delay time |
| $TI_1$, $TI_2$ | QUIPSS parameters |

# LIST OF ABBREVIATIONS

| | |
|---|---|
| MRI | Magnetic Resonance Imaging |
| DSC | Dynamic Susceptibility Contrast |
| ASL | Arterial Spin Labeling |
| CBF | Cerebral Blood Flow |
| rCBF | Regional Cerebral Blood Flow |
| CBV | Cerebral Blood Volume |
| MTT | Mean Transit Time |
| OEF | Oxygen Extraction Fraction |
| $CMRO_2$ | Cerebral Metabolic Rate of Oxygen |
| PET | Positron Emission Tomography |
| CT | Computed Tomography |
| PCT | Perfusion Computed Tomography |
| SPECT | Single Photon Emission Computed Tomography |
| BBB | Blood Brain Barrier |
| Hct | Hematocrit |
| BFV | Blood Flow Volume |
| ICA | Internal Carotid Artery |
| FOV | Field of view |
| WM | White Matter |
| GM | Gray Matter |
| CSF | Cerebrospinal Fluid |
| SNR | Signal-to-Noise Ratio |
| ROI | Region Of Interest |
| VOI | Volume Of Interest |
| SVD | Singular Value Decomposition |
| MT | Magnetization transfer |
| RF | Radio-frequency |
| FID | Free Induction Decay |

| | |
|---|---|
| NEX | Number of Excitations |
| IR | Inversion Recovery |
| SR | Saturation Recovery |

# 1. Introduction

This work employs several MRI techniques for cerebral perfusion measurements.

Imaging techniques in all modalities differ by the physical observables that are used as the source of information (attenuation coefficient, spin relaxation constants, radiation activity etc.) and the carrier of information (ultrasonic waves, electromagnetic waves etc.), the nature and type of contrast agents, the physiological model that couples the measured physical quantities with related physiological parameters, the accuracy of quantification, spatial resolution, brain coverage, scan time and clinical applications.

The term "perfusion imaging" is used for the determination of the parameters related with flow of nutrients to the tissues in interest. In this context, it is commonly used for the determination of cerebral blood flow (i.e. the volume of blood that flow to the volume of tissue in a given time). It is used with the unit ml/100g.1min in MRI.

For routine clinical use, an ideal method would assess the related physiological parameters with perfect accuracy in least possible time and also it could be applied to all cases. But in reality, every technique has advantages and disadvantages that have to be taken into account by the clinicians.

This work will focus on dynamic susceptibility contrast MRI (DSC-MRI) and arterial spin labeling (ASL). DSC-MRI will be used as the gold standard in both the qualitative and quantitative perspective in order to discuss the potential improvements in ASL. Quantitative imaging is the accurate determination of physiological parameters (in terms of predefined units) and has a big advantage over qualitative techniques. It provides better opportunities for intersubject comparisons. Technical knowledge and careful implementation of ASL technique will determine obtained accuracy of quantification, which will be investigated in the following parts of this thesis.

In this thesis, cerebral perfusion measurements were done in human subjects using ASL and DSC techniques of MRI. The experiments were divided into two parts; volunteers and patient scans. Perfusion is measured in terms of both ASL and DSC in patients, whereas only ASL technique is used for volunteers. The obtained quantitative values of perfusion in ASL, are compared with normalized results of DSC method and the standard perfusion values given in literature.

In the following parts, both techniques will be investigated in detail, and possible improvements will be discussed. But, before the detailed discussion of these MRI methods, in the following chapter, brief and subject related information about brain physiology and anatomy is given. In the third chapter, the perfusion imaging techniques in non-MRI modalities are introduced. The physiological models underlying perfusion measurements will be briefly presented in the fourth chapter. The discussion of MRI starts at chapter five, where the basic knowledge about the image formation mechanisms and signals in MR is given. In the sixth and seventh chapters DSC and ASL techniques are investigated in detail. In the eighth part, the results obtained by DSC and ASL techniques will be presented and discussed. The segmentation of brain into its tissue types is a part of perfusion imaging in ASL, so it is embedded in the "Results and Discussion" chapter.

# 2. Brain

Brain is the main information-processing unit of the body. In this chapter, a general information about brain anatomy and function will be given. Because the aim of this thesis is to measure cerebral perfusion, it would be helpful to start with the brain circulation and the properties of the blood.

## 2.1 Anatomy and Function

Brain consists of three basic parts: the forebrain (prosencephalon), midbrain (Mesencephalon), and hindbrain (Rhombencephalon).

Telencephelon is a part of forebrain, usually referred as cerebrum and divided into two hemispheres, left and right. The hemispheres are linked by large bundle of nerve fibers, named corpus callosum and by smaller commissures.

Outermost layer of the cerebrum is called cerebral cortex which has a thickness of 2-4 mm's. It is made up of gray matter which consists of nerve cell bodies, dendrites, glial cells and capillaries. The main role of cortex is to receive and process the information from sense organs. It has also complex brain functions as memory, attention and language. These functions were distributed to four lobes: frontal, parietal, temporal and occipital lobes of the cortex. The surface of cerebral cortex is folded, it contains ridges (gyri) and valleys (sulci) which are drawn in Figure 2.1.

White matter is another main tissue type in brain which is just the myelinated axons of the nerve cells. It is positioned medial of gray mater in cerebrum and connects various gray matter areas.

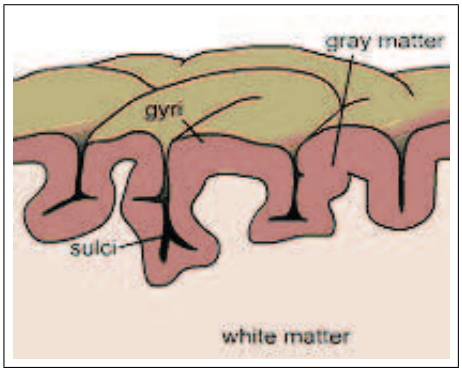


**Figure 2.1** Structure of cerebral cortex with white and gray matter distribution The cortex is a folded surface which consist of sulci and gyri [1].

## 2.2 Circulation

Brain circulation system carries oxygenated blood, glucose and other nutrients to the brain through the arteries and removes deoxygenated blood, carbon dioxide, lactic acid and other waste products via the veins.

Arteries carry the blood to the region, and then narrow forming arterioles and capillaries. Capillary is the site of circulation where the tissue is perfused. In the following subsections, the formation of the arterial system will be represented and the tissue perfusion will be described.

**2.2.0.1 Arterial Circulation.** Brain circulation is maintained by the branches of common carotid artery in the neck and subclavian artery which also supplies shoulders, lateral chest and arms (Figure 2.2).

Two internal carotid arteries, which branch from common carotid artery, and additionally, two vertebral arteries are branched from subclavian artery are the major arteries that supply blood to the brain. Within the cranium, the two vertebral arteries unite to form the basilar artery.

Right and left carotid arteries are interconnected via the anterior communicating

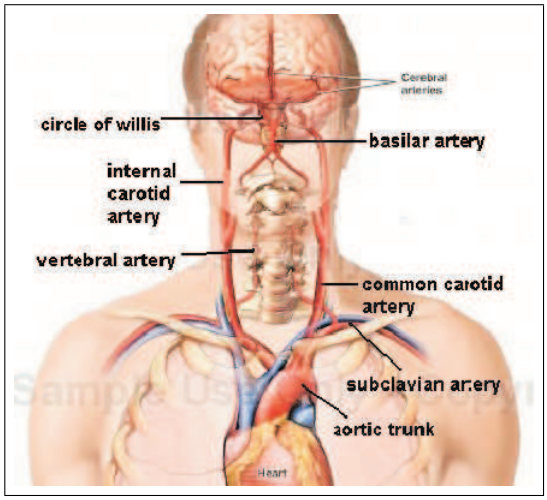


**Figure 2.2** Major arteries of the head [2].

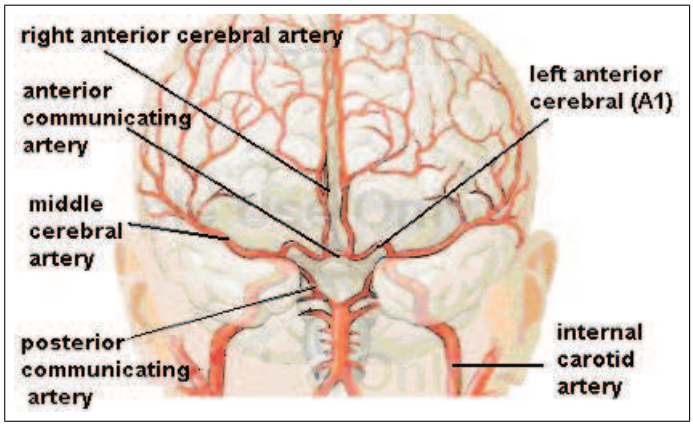


**Figure 2.3** Major arteries of the brain [2].

artery, and are connected with the basilar artery via bilateral posterior communicating artery. Basilar artery and both carotids with these communicating arteries form the circle of Willis, which is below the hypothalamus. It is the origin of anterior, middle and posterior arteries which supply the cerebral cortex (Figure 2.3).

**2.2.0.2 Capillary Circulation.** Capillary exchange enables the interchange of water, oxygen and many other nutrients then collects carbon dioxide and waste chemical substances in the venule end of capillaries from surrounding tissue. Then capillaries widen to form venules and the draining veins (Figure 2.4).

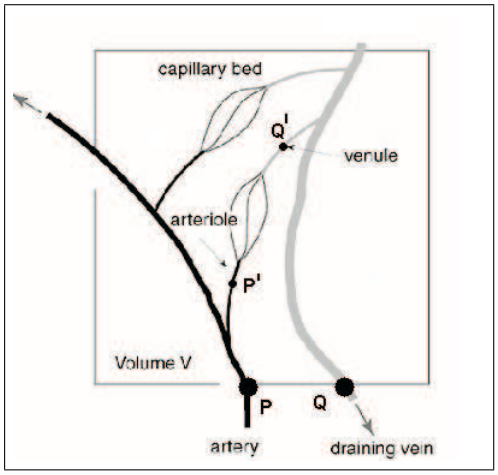


**Figure 2.4** Vascular structure of the volume of perfusion. Points are put on the pathway of circulating blood; P on the artery, P', Q' on the arteriole and venule respectively, Q on the vein.

The walls of brain capillaries consist of a continuous layer perforated only by tight junctions. Blood-brain barrier (BBB) is formed because of the tight junctions between the endothelial cells in the brain. It prevents large proteins from entering the brain and slows the penetration of smaller molecules. Diffusion and vesicular transport of materials across the capillaries is limited, but there are numerous active transport systems. Water, $CO_2$ and $O_2$ penetrate the capillaries easily. Glucose, as the source of energy for nerve cells, is transported across the capillaries by transporter GLUT1 [12]. Additionally, astrocytes contact the endothelial cells and contributes the targeted material exchange.

BBB is an additional defense mechanism which stabilize the neuronal environment, protect brain from endogenous and exogenous toxins in the blood, because of the sensitivity of neurons to ionic and material changes of the immediate environment.

## 2.3 Properties of Blood

Blood is the carrier of necessary materials to the tissue and collector of the waste products. It consists of fluid called plasma, and the former cells - red cells (erytrhrocytes), white cells (leukocytes), and platelets (thrombocytes) - which are suspended in

the plasma.

It is possible to measure the fractional volumes of these parts by centrifuging a sample volume in a test tube at low speed. Heavier red cells will be packed at the bottom of the tube, and plasma can be seen as a pale-yellow fluid above them. A thin layer of white cells and platelets is also seen in the tube.

The ratio of the total volume of erythrocytes to the total volume of blood is defined as hematocrit (Hct). In adult males, the average venous blood hematocrit was measured around 0.47 (in female, 0.42) [13]. But the hematocrit is not uniform through the arteries, capillaries and venules. In large vessels, the surface area to volume ratio is smaller than the tiny capillaries and arterioles; because of axial streaming of blood cells in vessels, red cells have tendency to flow in the medial of vessels, so the equal volume of blood in large vessels contain more red cells than the capillaries, resulting in higher hematocrit. Leukocytes and platelets are negligible because of low relative volume.

Additionally a discrepancy between the total body hematocrit and venous hematocrit and reported by Meier and Zeirler [3]. Authors discuss that, because of the venous blood is sampled along collecting catheter, the measured hematocrit depends on the ratio of the flow rates of blood plasma and erythrocytes. However, to calculate the volume of plasma and erythrocytes in a volume of flowing blood, one must assess the mean traversal times of both types with separate markers. When mean traversal time of plasma is taken 1.15 times of the erythrocytes' (because erythrocytes are observed to be faster than plasma), %40 venous hematocrit would yield K=0.92, where K is the ratio of blood volume hematocrit to venous hematocrit.

Blood plasma includes mineral ions (sodium, potassium, calcium and chloride), small organic molecules (e.g amino acids, fatty acids and glucose) and plasma proteins (albumin, globulin and some clotting factors). Ionic components maintain osmolality and pH within physiological limits. In normal healthy individuals, 7-9 percent of the plasma is made up of plasma proteins [13].

Erythrocytes are most numerous cell types in the blood volume, major function of which is to transport oxygen and carbon dioxide around the body. They are small, biconcave discs, have large area to volume ratio, thus permitting efficient particle exchange. The principal protein constituent of its cytoplasm is hemoglobin, which has oxygen binding function.

Leukocytes are mobile units of our protective immunologic system, which are large in size but smaller in number. Platelets have roles in control of bleeding and in the maintenance of integrity of the vascular endothelium.

Because of that the cerebral blood flow is measured by using endogenous and exogenous contrast agents of the blood plasma, the contents of this chapter will be used as a background information related with all the remaining chapters of the thesis.

# 3. Perfusion Imaging with Non-MRI Techniques

There are various imaging modalities that give information about brain hemodynamics. Because this thesis will focus on the MRI methods, these modalities were classified as MRI and non-MRI techniques. In this chapter non-MRI modalities will be introduced in terms of perfusion imaging.

## 3.1 Positron Emission Tomography (PET)

PET is a technique that provides quantitative information of regional cerebral blood flow (rCBF), regional cerebral blood volume (rCBV), regional oxygen extraction fraction (rOEF) and regional cerebral metabolic rate of oxygen ($rCMRO_2$) -or glucose-. These parameters are imaged by using various contrast agents which are sources of positron radioisotopes. $^{15}O_2$, $C^{15}O_2$, $H_2{}^{15}0$ are generally used PET tracers ($^{15}0$ has short half-life: 123 seconds [14]) [1] .

$H_2{}^{15}0$ is intravenously injected, positrons are produced by the decay of these isotopes of the agent and coincidence detection gamma-rays are used as the source of information. Kety-Schmidt model (Chapter 4.2) is used with the results of scan where arterial blood samplings were taken as an input. $H_2{}^{15}0$ is not a freely permeable, but has some advantages over alternative tracers which has greater blood-brain permeability and longer-lived radionuclides (e.g C-11 butanol). It is easily and reliably synthesized [16], it has effective half-life permitting 1-2 minutes scan time and has vanishing activity after measurements [17].

$^{18}F$ fluorodeoxyglucose can be used to measure the regional glucose consumption of the living tissues and also in the evaluation of cancer through whole body scanning. [15].

[1] Half-lives of other isotopes used in PET: $^{18}F$ 1.7 hours, $^{13}N$ 10 minutes, $^{11}C$ 20 minutes [15]

PET is accepted as gold standard in CBF imaging. But, underestimation of mean gray matter CBF is reported because of partial volume effect which stems from interference of gray matter signals with signals from white matter and cerebrospinal fluid. This is a direct result of relatively low in-plane resolution of PET (5-7.5 mm in-plane, in comparison to ASL with 2-4.5 mm in-plane resolution) [18].

## 3.2 Single Photon Emission Computed Tomography (SPECT)

SPECT generates tomographic images which show 3D-distribution of specific radiopharmaceuticals. Imaging of CBF is one of the major applications of SPECT.

It is not possible to label water with a single photon emitting compound. So, only indirect measurement of blood flow can be obtained [19]. $^{133}$Xenon was mostly used tracer for measuring brain hemodynamic in the past. But in daily clinical usage it is replaced by three alternatives: $^{99}$Tc labeled hexamethylpropylenamine oxime ($^{99}$Tc-HMPAO), $^{99}$Tc-Bicisate (ethyl cysteine dimer [ECD]), and $^{123}$I inosine-5-monophosphate ($^{123}$I-IMP).

Data processing relies on the microsphere principle for the $^{99}$Tc tracers and the Kety-Schmidt model for the $^{133}$Xenon and $^{123}$I-IMP, leading to the calculation of rCBF maps [15].

The main indications for SPECT studies are neuropsychiatric disorders (major depression, stress disorder, schizophrenia), neurodegenerative disorders (Alzheimer, Parkinson's disease) and presurgical localization of epileptic foci [15, 20].

## 3.3 Perfusion Computed Tomography (PCT)

Computed Tomography (CT) is an imaging modality, in which the collimated x-ray beams are used as the carrier of information. Contrast mechanism depends on attenuation of beams while passing through the tissue. As a result, CT is primarily related to the tissue density. This is why it is a good choice for studying the bone pathologies, but is not a useful modality in distinguishing white and gray matters of brain tissue. To increase tissue contrast, external agents can be introduced that changes the local attenuation values. Iodinated contrast materials are usually used for that purpose.

Perfusion Computed Tomography (PCT) is an extention of the conventional head CT scan, which takes a few minutes. Iodinated contrast material is administrated via the arm vein and stays in the vascular compartment. One image per second is taken by cine scanning during a total scanning time of 40 to 45 seconds [15]. CBF can be estimated by rate-of-upslope analysis of response curve or deconvolution analysis [21]. CBF, CBV and mean transit time (MTT) maps are obtained after the analysis. The comparison of these parametric images between abnormal regions and control regions give information about the alterations in brain hemodynamics in the related tissues. The disadvantage of PCT is restricted brain coverage [22].

## 3.4 Xenon-Enhanced Computed Tomography (XeCT)

XeCT has been used to obtain quantitative CBF in humans. It is accepted as gold standard when compared with PCT [23]. Xenon gas is inhaled as a contrast agent, it rapidly dissolves in blood, freely crosses the lipid-rich blood-brain barrier, and enters the brain.

Xenon is directly measured by the CT scanner. Kety-Schmidt model was used, the time course of the concentration of Xenon in the blood and brain is used, CBF and

the blood-brain partition coefficient ($\lambda$) for Xenon is calculated. However, Xenon may be harmful, side effects were seen in some scans [23], and is currently not approved by the Food and Drug Administration (FDA) [21].

## 3.5 Doppler Ultrasound

It has limited spatial resolution but improved temporal resolution. It is non-invasive, so does not require contrast injection and involve radiation. Measurement of blood flow volume (BFV) in internal cerebral artery (ICA) can be used as extra information that is in correlation with CBF in the corresponding hemisphere.

Some errors may take place because of the vessel diameter and flow angle on measured flow velocities. Digital Doppler ultrasonography is used in combination with angle-independent dual-beam flow technology which is based on simultaneous usage of two beams with well known geometric configuration to overcome these problems [21].

BFV measurement in the ICA is also useful to detect the sudden response of physiologic system to various effects that influence local or global blood flow [21].

All the modalities that are used to measure brain perfusion are based on a physiological model. The selection of the model mostly depends on the properties of the agent used. MRI and the modalities described above (except Doppler ultrasound) uses basicly two models, which will be investigated in Chapter 4.

# 4. Indicator-Dilution Methods

In order to couple the measurable quantities of a given imaging modality with the physiological parameters in interest, a model is used. The model tries to be well-descriptive about the system. Because of real physiological systems are very complicated and usually have unknown properties, all the models use certain assumptions which simplifies the system.

For quantification of perfusion parameters, generally two distinct models are used, which differs in behavior of tracers while passing thorough the vasculature. In terms of magnetic resonance imaging (MRI), dynamic susceptibility contrast enhanced (DSC) technique use Meier-Zierler model, while arterial spin labeling (ASL) Kety-Schmidt model for quantification of perfusion, depending on the diffusivity of the tracer across the BBB. These will be explained in the following sections.

## 4.1 Meier-Zierler Model

This model describes the behavior of non-diffusible tracers, whether endogenous or exogenous (originates from the body or outside the body), through the cerebral vasculature [24]. Because of the blood brain barrrier (BBB), some large molecules are unable to cross to tissue side, so are collected in the venules and veins after passing thorough capillaries (Figure 4.1).

A diagram of the vasculature was given earlier in figure 2.4. If we use the same


**Figure 4.1** The pathway of non-diffusible tracers.

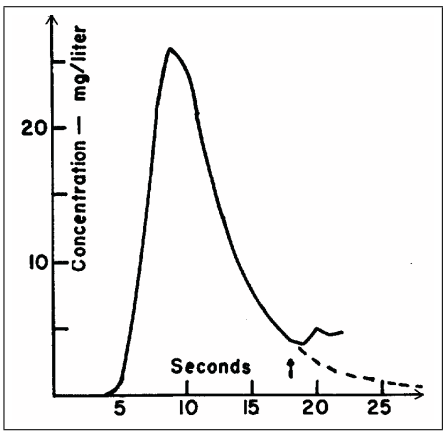


**Figure 4.2** Concentration of the tracer in vein. Also note that the pattern of traversal times of tracer particles h(t) is identical with the above graph, when the values in y-axis is multiplied by $\frac{F}{q}$. Arrow in the graph shows recirculation effect, where the concentration after the tracer passage does not return to zero [3].

notation for point locations, the indicator (tracer) is injected from the point P, and the concentration of the tracer in the blood is measured in point Q.

Let V be the volume of the vasculature between the points P and Q. q is the volume of indicator injected instantaneously at time zero. Measurements are performed by taking blood samples in the vein in various times. The measured concentration is the ratio of indicator volume and total blood volume, and denoted by c(t). The pattern of c(t) can be seen in figure 4.2.

This model has some assumptions [3]:

1. System is time-invariant. Flow and the velocity of the particles does not change in time.

2. System is representative for all particles. Probability density of traversal times are same for all particles.

3. The system has no stagnant pools. The fluid anywhere in the vasculature is eliminated and replaced by flow.

4. Recirculation of the indicator is not present.

Blood flow (F) has units volume/time, so when multiplied with dt, it gives the differential volume, if again multiplied with c(t), it gives the differential volume of indicator leaving the vasculature from the venous side. The total amount of indicator will leave the system from zero time to infinity, one can write;

$$q = \int_0^\infty Fc(t)dt \tag{4.1}$$

And because of F is thought to be constant;

$$q = F\int_0^\infty c(t)dt. \tag{4.2}$$

So;

$$F = \frac{q}{\int_0^\infty c(t)dt} \tag{4.3}$$

Since q is known, if c(t) is sampled correctly, flow can be calculated.

All indicator particles enters the vasculature from the point P, but traverses different pathways until arriving to Q. Thus they stay different times in the vasculature; this phenomena introduces the time-distribution function for all particles (remember the assumption 2).

In this context, it will be convenient to introduce h(t) where;

$$h(t) = \frac{F.c(t)}{q} \tag{4.4}$$

h(t) can be described as the fraction of indicator injected at time zero and leaving the system at time t. Because of its unit is 1/time, it is also named as the frequency function of traversal times [2] . A particle which has a traversal time t and flow F, possesses a volume t$\times$ F in the vasculature. If we define the differential volume; dV = t.F.h(t).dt, the total volume will be the integral of the volumes of particles which

[2] Note that h(t) is normalized; $\int_0^\infty h(t)dt = 1$ (4.5)

has traversal times from zero to infinity:

$$V = \int_0^\infty tFh(t)dt = F\int_0^\infty th(t)dt \tag{4.6}$$

The above equation leads to the central volume theorem;

$$V = F.\bar{t} \tag{4.7}$$

where $\bar{t}$ is the mean of the traversal times, also generally named as mean transit time and denoted as MTT[3] . In this context, it will be useful to mention that, the instantaneous injection of the indicator is not possible, so a function i(t) that describes the rate of injection must be defined. Briefly, i(t) is the volume of indicator that is injected to the artery at t. Then, the rate at which the indicator is leaving the system F.c(t) will be;

$$F.c(t) = \int_0^t i(t-s)h(s)ds = i(t) \otimes h(t) \tag{4.9}$$

where $\otimes$ denotes the convolution operator.

The parameters of the model and the units of the parameters are designed with respect to measurables of the experiment. In the first applications of this model, the volume of vascular bed is measured by using the arterial injection volume and concentration of the indicator in the venous side in various times.

However, in MRI, the signal is acquired from the voxel which contains the capillaries and the tissue compartments. So, it is more important to determine the concentration of the tracer (or indicator) in the capillary bed, rather than the venous or arterial side. For that purpose, instead of h(t), a residue function

$$R(t) = 1 - \int_0^t h(s)ds \tag{4.10}$$

is introduced, which gives the fraction of injected tracer still present in the vasculature

[3] Notice; $\bar{t} = \int_0^\infty th(t)dt = \frac{\int_0^\infty tFc(t)dt}{q} = \frac{\int_0^\infty tc(t)dt}{\int_0^\infty c(t)dt}$ (4.8)

at time t [25]. The amount of indicator in arterial and capillary side is measured in terms of concentrations ($C_a$ and $C_{VOI}$), so beside the dimensionless residue function (R), cerebral blood flow (CBF) is used with the unit of volume/(volume.time).

Concentration of the tracer in the voxel $C_{VOI}$ can be written as;

$$C_{VOI} = CBF \int_0^t C_a(s)R(t-s)ds = CBF.(C_a(t) \otimes R(t)) \tag{4.11}$$

In DSC-MRI, $C_a$ and $C_{VOI}$ are measured in terms of the measurables of MRI (i.e magnetic susceptibility differences), then deconvolution is performed to obtain F.R(t), which is used to determine F and calculate cerebral blood volume (CBV) and mean transit time (MTT). In the brain, the cerebral blood volume (CBV) is about 6% in the gray matter and 2-3% in the white matter [26], additionally Gd-DTPA agent has MTT of a few seconds [9]. This measurement process will be employed in the following parts of the thesis.

## 4.2 Kety-Schmidt Model

This model describes the behavior of diffusible tracers during passage through the vasculature and perfusion of tissue (Figure 4.3. It originates from the Fick's principle [4] . With an additional assumption that concentrations of the diffusible tracer in the vein and tissue reach equilibrium, the flow and partition coefficient parameters are derived; it will be analyzed next.

The original method and parameters were as follows: The diffusible low concentration nitrous oxide gas ($N_2O$) was inhaled by unanesthetized man, $N_2O$ concentrations were measured in artery and internal jagular vein for a ten-minute period from the beginning of the inhalation (Figure 4.4). The measured data was used to determine blood flow quantitatively [27, 4].

[4]Fick's principle has a usage of determination of cardiac output using the concentration measurements of $O_2$ and $CO_2$ in the artery and vein.

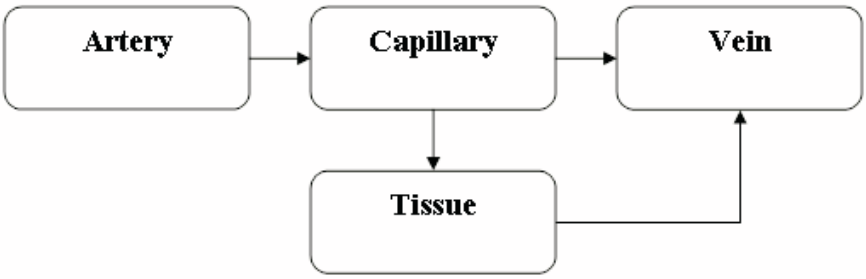


**Figure 4.3** The pathway of diffusible tracers in the vasculature.

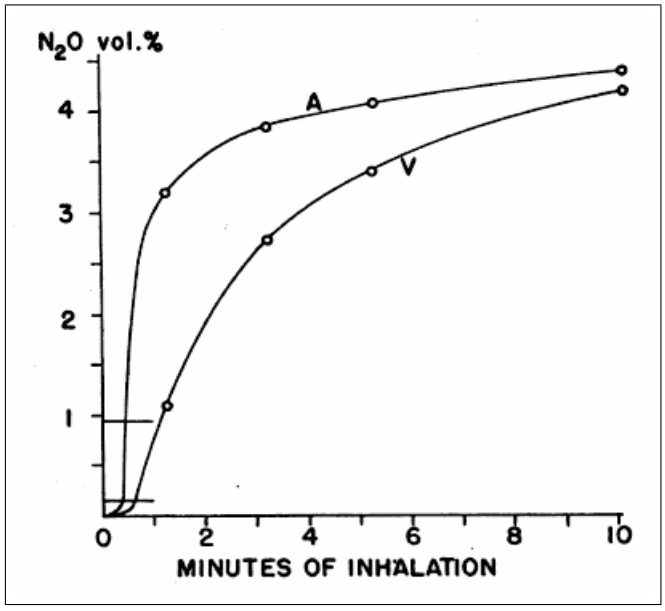


**Figure 4.4** Measurements of $N_2O$ concentration in artery and jagular vein during the start of inhalation [4].

Using the following notation:

| | |
|---|---|
| $V_{total,t}(t)$ | Total quantity of tracer ($N_2O$ in this case) uptaken by brain up to time t. It has units of volume. |
| $V_{total,a}(t)$ | Total quantity of tracer carried by artery to the brain up to time t. It has units of volume. |
| $V_{total,v}(t)$ | Total quantity of tracer removed by vein from the brain up to time t. It has units of volume. |
| $C_a(t)$ | Arterial tracer concentration at time t. |
| $C_v(t)$ | Venous tracer concentration at time t. |
| $C_t(t)$ | Tissue tracer concentration at time t. It has units of (volume of tracer in brain)/(weight of brain) |
| TF | Total cerebral blood flow. It has units of (volume of blood)/time. |
| CBF | Cerebral blood flow. It has units of (volume of blood)/(weight of brain . time). |
| $\lambda$ | Tissue-blood partition coefficient. Describes the distribution of the tracer between blood and tissue in equilibrium state. It has units of (volume of tracer)/(weight of brain). |
| W | Weight of the brain. |

Fick's principle states that;

$$\frac{dC_t(t)}{dt} = CBF.C_a(t) - CBF.C_v(t) \tag{4.12}$$

which is also equivalent to:

$$V_{total,t}(t) = V_{total,a}(t) - V_{total,v}(t) \tag{4.13}$$

Then,

$$V_{total,t}(t) = TF \int_0^t [C_a(t) - C_v(t)].dt \tag{4.14}$$

$$TF = \frac{V_{total,t}}{\int_0^t [C_a(\tau) - C_v(\tau)].d\tau} \tag{4.15}$$

Dividing both sides by W, we obtain

$$\frac{TF}{W} = \frac{V_{total,t}/W}{\int_0^t [C_a(\tau) - C_v(\tau)].d\tau} \tag{4.16}$$

$$CBF = \frac{C_t(t)}{\int_0^t [C_a(\tau) - C_v(\tau)].d\tau} \tag{4.17}$$

If t is long enough [5] that the arterial, tissue and venous concentrations reach equilibrium, $C_t(\infty) = \lambda.{}_a(\infty) = \lambda.C_v(\infty)$. By substituting this property, and multiplying both sides by 100, we obtain CBF in terms of 100 g. of brain tissue (which is generally used in the literature) and equal to;

$$CBF = \frac{100.\lambda.C_v(\infty)}{\int_0^\infty [C_a(\tau) - C_v(\tau)].d\tau} \tag{4.18}$$

In brief, $C_a$ and $C_v$ is measured at multiple times and in equilibrium condition, while $\lambda$ is determined in vitro [27], CBF can be calculated.

However, in terms of MRI, the signal is not acquired only from the arterial and venous side but also from the capillary and tissue side. So, the principles above is used and modified for the quantification of CBF using arterial spin labeling (ASL) technique, which uses water as an endogenous diffusible contrast agent. Because a free diffusible tracer is used, there is no access to the blood volume [26], but ASL provides acceptable quantified CBF values for brain perfusion imaging. The details will be discussed in the related parts of the thesis.

[5] In $N_2O$ experiments it is nearly 10 minutes [27].

# 5. Nuclear Magnetic Resonance (NMR)

## 5.1 Principles

A nuclear magnetic resonance (NMR) active nuclei has a non-zero magnetic moment, $\overrightarrow{\mu}$. When it is put in an external magnetic field $\overrightarrow{B_0}$, it starts precessing around the direction of $B_0$ (also named z-direction or longitudinal direction in MRI literature). The angular frequency of precession $\omega$, is given as;

$$\omega = \gamma.B_0 \tag{5.1}$$

where $\gamma$ is a constant named gyromagnetic ratio.

Every nuclei has a specific spin quantum number, which is denoted as I. The importance of I is that, there are 2I+1 possible orientations of $\overrightarrow{\mu}$ with respect to $\overrightarrow{B_0}$ [28]. This orientations determine longitudinal and transverse components of $\overrightarrow{\mu}$, denoted as $\overrightarrow{\mu_z}$ and $\overrightarrow{\mu_{xy}}$. These moments or spins, are in different energy states when they are in different orientations.

If a group of spins is in consideration, the total magnetic moment or the net magnetization $\overrightarrow{M}$ is calculated as;

$$\overrightarrow{M} = \sum_{n=1}^{N_s} \overrightarrow{\mu_n} \tag{5.2}$$

where $N_s$ is the total number of spins [28]. Additionally, the net magnetization is along the z-direction. When $B_0$ is applied, the projection of $\mu$'s on transverse plane has random phases. So $M_z^0$ can be used to emphasize the net equilibrium's z-directional magnetization instead of $\overrightarrow{M}$ in some cases.

The distribution of spins in these energy states is described by Boltzmann rela-

tionship, so the net magnetization can be derived as [28],

$$M_z^0 = \frac{\gamma^2 \hbar^2 B_0 N_S I(I+1)}{3KT_S} \tag{5.3}$$

where $\hbar$ is related to the Planck constant, K is the Boltzmann constant, $N_s$ is the number of spins and $T_S$ is the local temperature.

It is important to verify that the net equilibrium magnetization is directly proportional to the number of spins, which will be used in the determination of $M_{0B}$, described in Appendix D.

## 5.2 Excitation

The spin system has a net longitudinal magnetization - denoted as $M_Z^0$ or $M_0$ - in the equilibrium state.

If an oscillatory magnetic field $B_1$ - also named radiofrequency (RF) pulse - is applied in addition to the static $B_0$ field, the spin begin to precess around the new net magnetic field. This results in flipping of the net magnetization, which redistributes the longitudinal and transverse components of the $M_0$ determined by the flip angle $\alpha$.

The resonance condition must be present, if an external field is able to disturb the spin system. This can be described as, the energy of external electromagnetic field must match the energy difference between the states of spins. This is also called on-resonance excitation and extensively used for slice selection in MRI.

Also, in practice, unwanted off-resonance excitations may occur because of field inhomogeneities and chemical-shift effects.

## 5.3 Relaxation

After the spin system is disturbed, it starts to return to its original state. The recovery of longitudinal magnetization is called the longitudinal relaxation and described by the time constant $T_1$. If the RF pulse produced a net transverse magnetization after flipping, then this transverse magnetization will also return to its original value, zero. This loss of transverse magnetization is called transverse relaxation and described by the time constant $T_2$.

Transverse relaxation stems from the loss of phase coherence of spins in the system, so it is an intrinsic property [29]. However in the MRI systems there are field inhomogeneities produced by the main magnet and local tissue susceptibilities. These inhomogeneities enhance the transverse relaxation, if the effects are not eliminated. Then the apparent transverse relaxation constant, let denote it $T_2^*$, be calculated as,

$$\frac{1}{T_2^*} = \frac{1}{T_2} + \frac{1}{T_{2in}} \tag{5.4}$$

where $T_{2in}$ is the effective relaxation time due to only field inhomogeneities.

The time evolution of longitudinal and transverse relaxations are described as,

$$\begin{aligned} \frac{dM_{z'}}{dt} &= \frac{M_z^0 - M_{z'}}{T_1} \\ \frac{dM_{x'y'}}{dt} &= -\frac{M_{x'y'}}{T_2} \end{aligned} \tag{5.5}$$

which is derived from a general Bloch equation formulation [28].

The solutions of first order Eq.5.5 for longitudinal and transverse components are obtained as,

$$M_{z'}(t) = M_z^0(1 - e^{-t/T_1})M_{z'}(0_+)e^{-t/T_1} \tag{5.6}$$

$$M_{x'y'}(t) = M_{x'y'}(0_+)e^{-t/T_2} \tag{5.7}$$

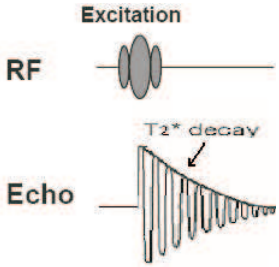


**Figure 5.1** FID signal.

where $M_{z'}(0_+)$ and $M_{x'y'}(0_+)$ are the longitudinal and transverse magnetizations just after the RF pulse.

If $\frac{\pi}{2}$ pulse is applied, the Eq.5.6 and Eq.5.7 become,

$$\begin{aligned} M_{z'}(t) &= M_z^0(1 - e^{-t/T_1}) \\ M_{x'y'}(t) &= M_z^0 e^{-t/T_2} \end{aligned} \tag{5.8}$$

and such behavior of spin system is named as saturation recovery (SR) relaxation.

If $\pi$ pulse is applied, the Eq.5.6 and Eq.5.7 become,

$$\begin{aligned} M_{z'}(t) &= M_z^0(1 - 2e^{-t/T_1}) \\ M_{x'y'}(t) &= 0 \end{aligned} \tag{5.9}$$

and such behavior of spin system is named as inversion recovery (IR) relaxation. This type of relaxation is used in ASL and segmentation analysis of ASL data.

During the relaxation period the net magnetization is not preserved, sice longitudinal and transverse relaxation are completely independent processes.

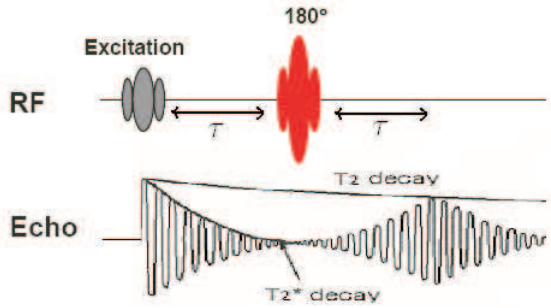


**Figure 5.2** Spin echo signal.

## 5.4 MR Signal

### 5.4.1 Free Induction Decay (FID)

FID is a transient signal which is the result of a single pulse on a spin system. When a transverse magnetization is obtained, at the initial time it has the maximum amplitude, then decays with time constant $T_2^*$ (Figure 5.1).

### 5.4.2 Spin Echo Signal

It consists of a $90^o$ pulse followed by (after a time delay $\tau$) $180^0$ pulse which rephase the spins and produce a signal maximum at $2\tau$. After the start of the excitation pulse, this time that response obtained with maximum amplitude is called the echo time, and denoted as $T_E$.

After the first excitation pulse, the transverse magnetization starts to decay with $T_2^*$, it means the field inhomogeneities are effective. However, $180^0$ pulse rephases the spins, and an echo is formed at time $2\tau$ or, $T_E$. Maximum amplitudes at the initial time and the echo time points produce an envelope which decays with $T_2$. So, the effects of field inhomogeneities are eliminated. Thus the obtained echo is $T_2$ weighted (Figure 5.2).

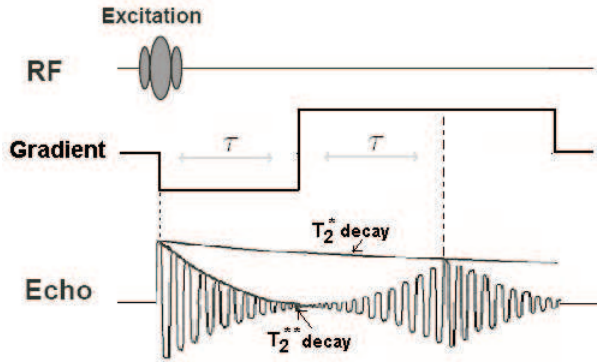


**Figure 5.3** Gradient echo signal.

### 5.4.3 Gradient Echo Signal

This form of echo signal is formed by varying gradient fields. Only one excitation pulse is applied, which is followed by gradient changes to phase and rephase the signal (Figure 5.3).

After the excitation pulse, the transverse magnetization would be subject to relaxation by $T_2^*$, but with simultaneously applied gradient, it will decay faster, say with the relaxation constant $T_2^{**}$. Then the negative gradient rephases the spins and produce an echo at $2.\tau$=$T_E$ again. Maximum amplitudes at the initial time and the echo time points produce an envelope which decays with $T_2^*$. It means that the obtained echo is $T_2^*$ weighted.

## 5.5 Echo Planar Imaging (EPI) Sequence

EPI is a fast acquisition method, that has the ability to form a complete image with a single excitation.

A typical MR image is formed from N repeated samples (phase encoding steps) in conventional sequences, such that each sample is taken in a $T_R$. $T_R$ is the time interval between the excitations, so the imaging time becomes (number of phase encoding

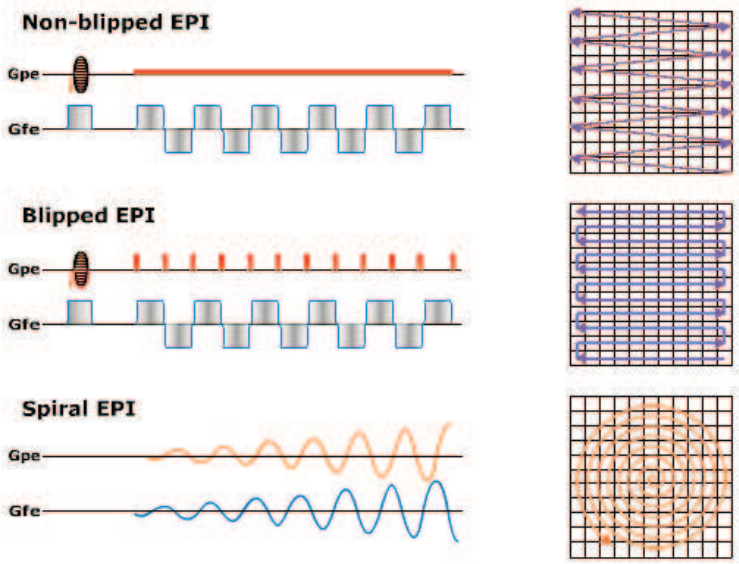


**Figure 5.4** Possible k-space sampling trajectories and corresponding sequence schemes in EPI [5].

steps)$\times T_R$ for those sequences.

By comparison, the EPI provides a significant decrease in scan times by collecting all of the image data in a single shot in 40 to 150 milliseconds, depending on hardware and contrast considerations [30]. Its disadvantage is the limited spatial resolution.

In EPI, the readout gradient is continuously applied during the sampling of k-space, while a phase encoding gradient is applied via small blipped or kept on continuously for cartesian imaging. But these result in different sampling trajectories of k-space (Figure 5.4). If both of the gradients are sinusoidal, then a spiral trajectory can be obtained.

In this thesis, DSC and ASL imaging will be obtained using EPI. Also, segmentation of the brain images was done using images acquired with EPI-based MR sequences.

# 6. Perfusion Measurements in DSC

DSC technique relies on the measurement of change in transverse relaxation time constant of the tissue, while the injected bolus of contrast agent passes through the vasculature.

In DSC, a chelate of Gadolinium, Gd-DTPA (Gadolinium diethylenetriamine-pentaacetic acid) is generally used. It is an intravascular agent, so cannot pass across the BBB.

The pathway of contrast agent after injection from a peripherical vein is as follows; it is carried to the heart, enters the pulmanory circulation, carried back to heart, enters the systemic circulation via the aorta, reaches to Circle of Willis in the brain and distributed to various parts of cerebral cortex (Figure 6.1).

## 6.1 Pulse Sequence

Gadolinium decreases the $T_1$ of the tissue, so increases the tissue signal in $T_1$-weighted image. Additionally, as the bolus of Gd-DTPA passes through the vasculature, as a paramagnetic material, it produces magnetic susceptibility difference between the intravascular and extravascular compartments.

Magnetization and dynamic changes in magnetization can directly be measured by MRI. Magnetization before and during the full bolus passage has to be measured for quantification. To measure the effect of bolus passage on MR signal, $T_2^*$ weighted equilibrium magnetization must be acquired with fast scanning techniques. Generally, gradient echo (GE) or spin echo (SE) techniques are used with EPI acquisition for fast scanning with $T_R$ values lower than 2 seconds (usually $T_R$ between 1 and 1.5 second is used). This scheme also allows multi-slice imaging.

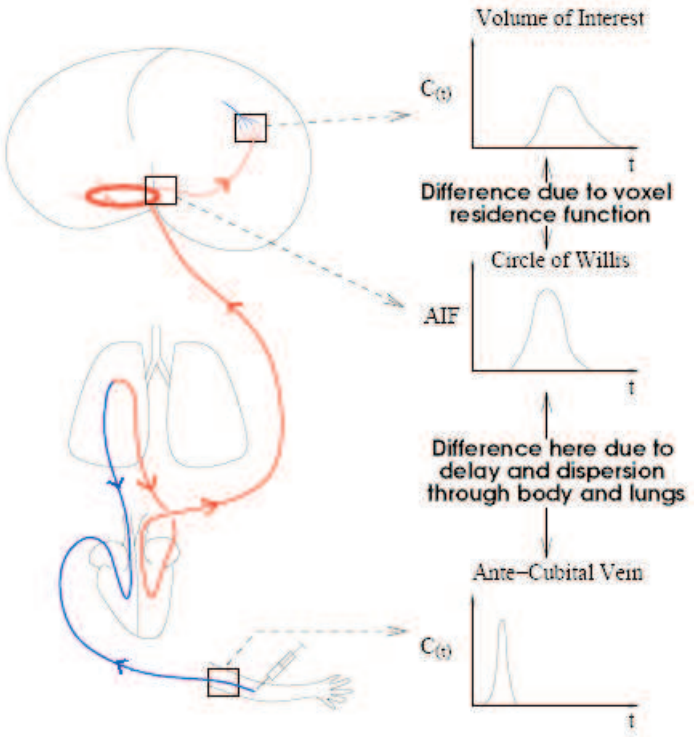


**Figure 6.1** The pathway of bolus from the injection site to the imaging plane [6].

Because of the enhanced inhomogenity, the spins next to the contrast agent loose phase faster, so decreased $T_2^*$ is observed in gradient recalled echo (GRE) sequences. Also, reduced $T_2$ is observed in spin echo (SE) sequences, because of diffusion along the field gradient, the spins are subject to irreversible losses of phase coherence. Dynamic susceptibility contrast (DSC) technique is based on measuring these susceptibility differences [29, 31].

## 6.2 Assessment of Perfusion Parameters from DSC Measurements

In the second step of perfusion determination, the measured magnetization values has to be coupled with the concentration of the agent and magnetic susceptibility effects. This is done by using,

$$C_{VOI}(t) = -\frac{k}{T_E} ln(\frac{S(t)}{S_0}) \tag{6.1}$$

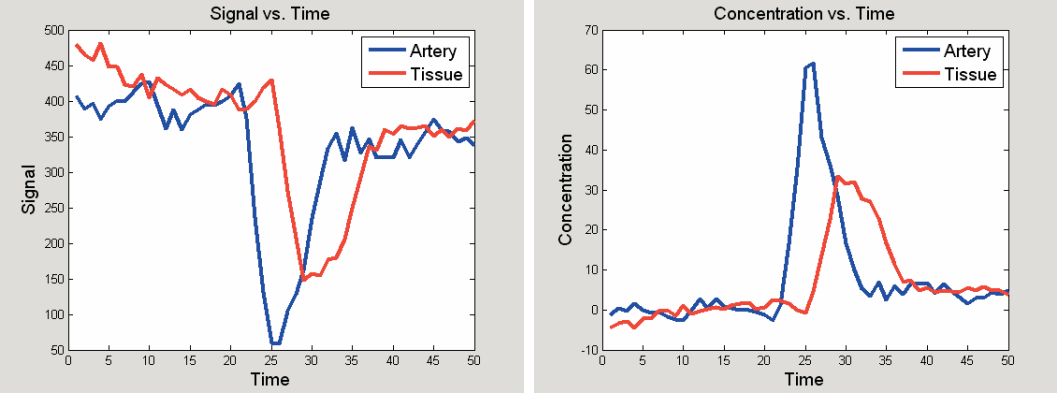


(a) (b)

**Figure 6.2** a) Measured signal before and during the passage of bolus from artery and tissue voxel is described in the figure. b) Signal measurements are converted to concentration values using Eq.6.1.

which is derived in Appendix A[6] . $S_0$ in Eq.6.1 denotes the baseline signal where S(t) is the measured signal in time t. So, total sampling time must include the baseline, from which the $S_0$ is calculated, and at least the first passage of bolus [7] .

The measured MR signals are used to obtain contrast agent concentration curves for each voxel. In the following part, these curves will be used to obtain perfusion parameters.

Meier-Zierler model is used to describe the concentration of the non-diffusible Gd-DTPA in the tissue (Chapter 4.1). In DSC-MRI technique, the signal is acquired from the region of interest which includes capillaries, so the model is used with residue function R(t) defined in Eq.4.10 instead of h(t). Then the tracer concentration in the vasculature is modeled by using Eq.4.11.

Measurement process includes the assessment of concentration-time curves of every voxel. Among these voxels, the ones with fast tracer arrival and small FWHM in the artery sites can be averaged to be used as arterial input function $C_a(t)$, whereas the remaining voxels will be behaved as tissue concentration $C_{VOI}(t)$ (Figure 6.2).

[6] $S_0$ is used instead of $S_{pre}$ of Appendix D., because $S_0$ is found by averaging more than one signal measurements before the bolus passage. $C_{VOI}$ is the concentration of agent in the voxel, k is the calibration factor and $T_E$ is the echo time.

[7] Even if the recirculation of the agent is measured, it will be excluded in the further analysis.

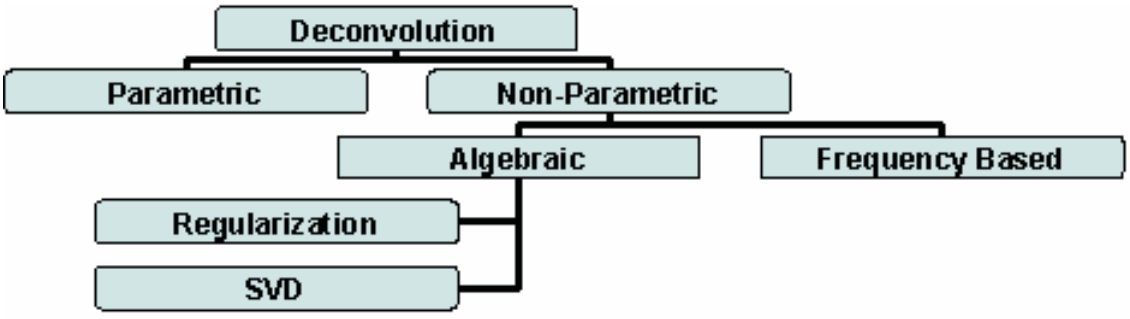


**Figure 6.3** Deconvolution methods.

Solving Eq.4.11 means deconvolution, where R(t) and the coefficient CBF are found as a result. However, this is inverse problem because of R(t) is unknown. Two types of approaches are used generally for solution, the former is the parametric approach (also named model dependent, analytical) where there is an assumed function for the shape of R(t). This is generally the exponential with the time constant equal to MTT [25]. The latter is the non-parametric approach (also named model-independent), where R(t) is found without a priori knowledge of the shape.

In this thesis, the non-parametric approaches will be emphasized. They are divided into two common approaches. The first one is the transform approach, where the Laplace, Z or Fourier transform is applied on the measurement results. There are some advantages of transformed data in terms of processing, for example convolution in time domain corresponds to multiplication in frequency domain [8] . A signal in time domain is transformed into frequency domain by Fourier transform (discrete Fourier transform in this context). However, non-parametric approaches are very sensitive to noise. For frequency based transform approaches described above, additionally a dedicated filter is applied to increase the weight of physiological signal over noise [25].

In a second approach of non-parametric methods, the time domain of the measured concentration signals are used. Again, Eq.4.11 includes convolution operator which is described as integral is used, however, because the measurement process is discrete in nature, the integral must be replaced by summation in order to adopt the

[8]Then, deconvolution of $C_{VOI}$ with $C_a$ in time domain means the division of $C_{VOI}$ with $C_a$ in frequency domain.

MRI context. If we assume the concentrations are measured at times $t_i$, $t_1$,..., $t_N$, then we obtain;

$$C_{VOI}(t_j) = CBF.\Delta t \sum_{i=1}^{N} C_a(t_i) R(t_j - t_i) \tag{6.2}$$

or

$$\begin{pmatrix} C_{VOI}(t_1) \\ C_{VOI}(t_2) \\ \vdots \\ C_{VOI}(t_N) \end{pmatrix} = CBF.\Delta t \begin{pmatrix} C_a(t_1) & 0 & \dots & 0 \\ C_a(t_2) & C_a(t_1) & \dots & 0 \\ \vdots & \vdots & \ddots & \vdots \\ C_a(t_N) & C_a(t_{N-1}) & \dots & C_a(t_1) \end{pmatrix} \begin{pmatrix} R(t_1) \\ R(t_2) \\ \vdots \\ R(t_N) \end{pmatrix} \tag{6.3}$$

as the equivalent discrete form of Eq.4.11. Eq.6.2 or Eq.6.3 will be used as the major equation in the subsequent parts of this section. R(t) and CBF is obtained by the deconvolution of $C_{VOI}$ with $C_a$.

Eq.6.2 or 6.3 can also be written in vector-matrix notation;

$$\mathbf{c} = \mathbf{A} \ . \ \mathbf{b} \tag{6.4}$$

where **c** and **A** contains the elements of $C_{VOI}$ and $C_a$ respectively, and **b** contains the elements of R(t) times CBF.$\Delta$t.

Because of the discrete nature, the concentration is sampled at various times, but measured concentrations are assumed to be constant between time points. This is however a poor assumption. Ostergaard et al.[25] offered to use the modified version of matrix **A** in Eq.6.4, where each concentration term is weighted with previous and next concentrations;

$$A_{ij} = \begin{cases} [C_a(t_{i-j-1}) + 4.C_a(t_{i-j}) + C_a(t_{i-j+1})]/6 & 0 \leq \text{j} \leq \text{i} \\ 0 & \text{otherwise} \end{cases} \tag{6.5}$$

Using the Eq.6.4, **b** is found as;

$$\mathbf{b} = \mathbf{A}^{-1}.\mathbf{c} \tag{6.6}$$

But the direct solution is subject to noise, so some algebraic methods for deconvolution are applied to solve Eq.6.7. Singular value decomposition (SVD) is one of these methods. For the solution, the matrix $\mathbf{A}$ is decomposed into $\mathbf{U}.\mathbf{W}.\mathbf{V}^t$, where $\mathbf{U}$ is m×n column orthogonal matrix, $\mathbf{W}$ is a n×n diagonal matrix with positive or zero elements and $\mathbf{V}$ is n×n orthogonal matrix.

A threshold is applied to the matrix $\mathbf{W}$. Among the diagonal elements $w_i$ which is lower than the maximal value of $w_i$ multiplied by the threshold value is set to zero.

Then $\mathbf{A}^{-1}$ can be written as $\mathbf{V}.\mathbf{W}^{-1}.\mathbf{U}^t$. As a result, Eq.6.7 becomes;

$$\mathbf{b} = \mathbf{V}.\mathbf{W}^{-1}.\mathbf{U}^t.\mathbf{c} \tag{6.7}$$

As a result, CBF.Δt.R(t) is obtained. Δt is a scan parameter and equal to $T_R$, R(t) is a decreasing function [9] (from 1 to 0). So, using the global maxima of the result of deconvolution, CBF is found.

Secondly, as described in Appendix B, MTT is equal to the integral of R(t).

Lastly, CBV can be calculated by two ways. First one is as described in Appendix B, by using the residue function R(t) with central volume theorem. Second way is the usage of concentration-time curve as follows;

$$CBV = \frac{\int_0^\infty C_{VOI} dt}{\int_0^\infty C_a dt} \tag{6.8}$$

which calculates the CBV in tems of concentration-time curves [10] .

Perkiö et al. compared four post-processing methods for that purpose using simulation and patient data [7]. As shown in Figure 6.4, first three methods rely on concentration-time curves, whereas the fourth one uses the residue function. In the

[9] For some pixels, it will be observed to increase in the beginning. The reason is the selection of arterial input function (AIF), which may not be accurate because of the dispersion of bolus from the selected site to the ideal site for real AIF.

[10] Mathematically, the integral of the convolution of two functions is equal to the multiplication of integral of each function. When this principle is applied to Eq.4.11, Eq.6.8 is obtained.

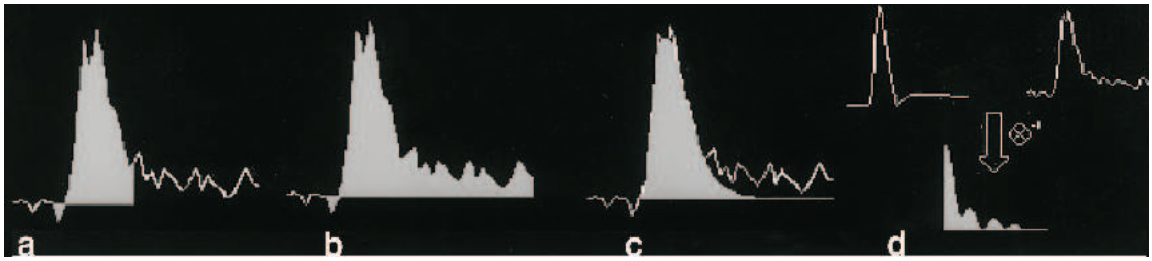


**Figure 6.4** Four postprocessing methods to determine CBV. a) Area is calculated using consecutive trapezoid areas. Time interval of integration is determined by the deviation from the baseline signal. It is aimed to eliminate the recirculation effect, which results in overestimation of CBV. b) Area is calculated using consecutive trapezoid areas in the full time interval. c) Area is calculated gamma variate fit. Again the prevention of recirculation effect is aimed. It is accepted a more robust way to determine CBV that the method in a. d) CBV is found by the multiplication of CBF with the area under R(t) in accordance with central value theorem [7].

same paper, it is also reported that; among the four methods, the one which uses the R(t) to calculate CBV provided the most accurate estimates of the simulation results.

The CBV calculations will be done by using R(t) in DSC part of this work.

# 7. Perfusion Measurements in ASL

Arterial spin labeling (ASL) is a non-invasive technique for perfusion measurements, in which the magnetically tagged arterial blood is used for endogenous tracer. The advantage of ASL-based perfusion techniques is to use an intrinsic contrast agent (blood) to quantify blood perfusion, eliminating the need of injection of external contrast agents.

ASL experiment consist of two parts; images were acquires both in the control and tag experiments. These experiments are designed to be weighted equally by the static tissue, but have different weights on flowing spins. So, after the subtraction of the control and tag images, the signals from static tissue are eliminated, and an uncalibrated map of flowing spins are obtained (Figure 7.1).

## 7.1 Pulse Sequence

There are different kinds of ASL sequences, they can be divided into two categories; continuous and pulsed ASL.

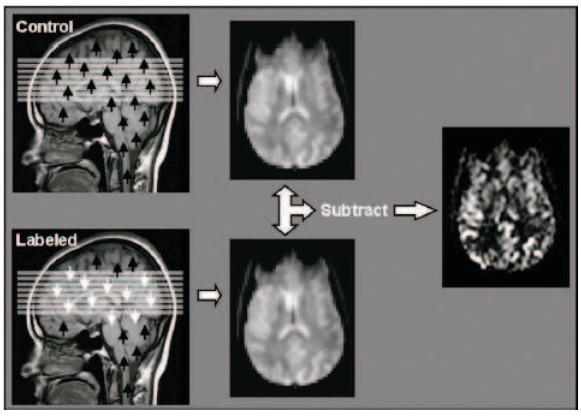


**Figure 7.1** The flowing spins are labeled during tag experiment. The subtracted image intensity is directly proportional to CBF [8].

### 7.1.1 Continuous ASL (CASL)

In CASL, the labeling of flowing spins is performed continuously in the neck. In the early works, labeling was done by saturation of the flowing spins, later inversion is used instead of saturation to enhance the contrast.

Arterial blood is inverted by constant low-power RF irradiation and the magnetic field gradient along the flow direction. The inverted spins after passing through the inversion plane, is subject to $T_1$ decay while moving towards imaging plane.

In the control image it is not enough to repeat the experiment without the inversion of the moving spins. Because the magnetization of the imaging slice is effected by continuous RF irradiation in terms of magnetization transfer (MT) effects. To overcome this problem, some methods are offered. One could design the control experiment with the inversion plane moved symetrically opposite side of the imaging slice. In this technique only one slice can be acquired. Another method is using separate RF coils for inversion and imaging. This allows multislice imaging, but requires specialized hardware [9].

### 7.1.2 Pulsed ASL (PASL)

Unlike the CASL, in PASL, the spins are inverted by short duration (10-15 ms) inversion pulses. Inversion is performed in a volume of flowing spins, rather than a thin slice like in the case of CASL.

Elimination of the static tissue after the subtraction of control and tag images is expected. For that purpose, a saturation pulse is applied to the imaging slice just before the inversion pulse in some sequences. This reduces the signal coming from the tissue.

There are different techniques for PASL, which use various strategies in designing

the control and tag experiment, in terms of RF properties and the localization of inversion or saturation planes. In the following subsections some of these techniques will be described briefly, their advantages and disadvantages will be stated.

In PASL, images were collected both in the control and tag experiment. There is a time gap between the inversion pulse and the imaging pulse, which is named delay time and denoted as TI.

**7.1.2.1 EPISTAR Sequence.** EPISTAR (Echo-Planar Imaging and Signal Targeting with Alternating Radiofrequency) sequence is as follows.

In the tag experiment, the flowing spins are inverted in a volume (or slab) proximal to the imaging slice. There is a spatial gap between the inversion volume and imaging slice. This is preferred because of imperfect inversion slice profiles that may potentially disturb the spins on the imaging slice.

When the inversion pulse is applied, inverted arterial spins move towards the imaging slice and simultaneously be subject to $T_1$ decay. After the delay time TI, imaging pulse is applied on the imaging slice, where the magnetizations of the flowing spins and local spins are measured.

In the control experiment, inversion is applied to the opposite side of imaging plane symetrically to overcome MT effects (Figure 7.2). This is equivalent to the pulsed form of CASL described above. After the same delay time, imaging pulse is applied on the imaging slice again [32].

The subtraction of the two images results in elimination of the static tissue signal in ideal conditions, yielding a perfusion weighted image.

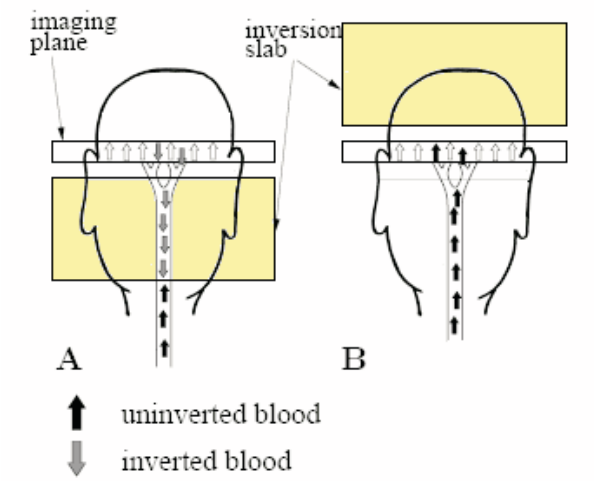


**Figure 7.2** EPISTAR Sequence [9].

**7.1.2.2 PICORE Sequence.** PICORE (Proximal inversion with a Control for Off-Resonance Effects) sequence differs from EPISTAR only in the control experiment. PICORE copes with MT effects by using off-resonance non-selective inversion pulse such that the frequency offset is identical with tag experiment's [33].

**7.1.2.3 TILT Sequence.** In TILT (Transfer Insensitive Labeling Technique) sequence, two consecutive $\frac{\pi}{2}$ pulses are applied to the inversion volume instead of inversion pulse. In the control experiment, again $\frac{\pi}{2}$ pulses are applied to the same slice with opposite phases. TILT provides good MT control, however it uses longer tagging pulses which is disadvantageous [34].

**7.1.2.4 FAIR Sequence.** FAIR (Flow-Sensitive Alternating Inversion) sequence consists of control experiment with slice selective (ss) inversion and the tag experiment with non-selective (ns) inversion (Figure 7.3. The difference of the obtained images in both experiments is flow weighted [35].

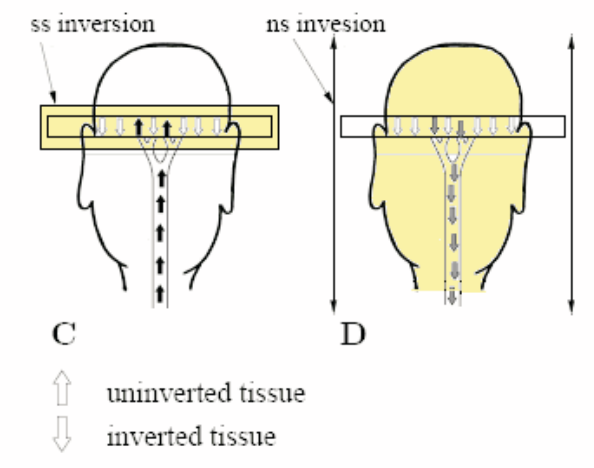


**Figure 7.3** FAIR Sequence [9].

### 7.1.3 Modifications of PASL Sequences

In this and the following sections, the term PASL will be used referring EPISTAR or PICORE sequences rather than FAIR. Because FAIR is different in nature, quantification of perfusion in FAIR is based on $T_1$ method which is different than the other quantification methods.

Unlike CASL, inversion pulse in PASL is applied in spatial domain. This means that the temporal width of the bolus of inverted blood is unknown at the first stage. It is denoted as $\tau$. For quantification, this parameter must be determined or controlled.

It is previously stated that, there is a spatial gap between the inversion and imaging volumes. This introduces a time gap for inverted blood to reach the imaging slice. This gap is named transit delay (or transit time) in ASL literature and denoted as $\delta$t (or $\Delta$t).

CBF is used with the unit $\frac{volume}{volume.time}$, so the volume of blood that passed until time t is CBF$\times$t if the transit delay is ignored. Just after tagging, the difference of control and tag magnetization of the arterial spin become $2M_{0B}$, if we assume there is no $T_1$ decay, the net magnetization carried to the imaging slice by inverted bolus of spins will be $2.M_{0B}$.CBF.t. This is identical to the microsphere method [31], i.e. the

spin reaching to the capillary of the imaging slice is trapped there. Since water is used as endogenous tracer in ASL and is diffusible, the clearence of water from the venous side in ASL scanning time duration is negligible.

If the signal from static tissue is suppressed, then the magnetization difference between the control and tag experiments become;

$$\Delta M(t) = 2.M_{0B}.CBF.t \tag{7.1}$$

If the $T_1$ decay is taken into account, until the blood reaches to the capillaries the tagged spins decay with the $T_1$ of the blood ($T_{1B}$), then start to decay with the $T_1$ of the tissue after exchanging from blood to the tissue. $T_1$ decay of the blood described in the following equation and if the $T_1$ shift and venous clearence is lumped into the term q, then Eq.7.1 becomes;

$$\Delta M(t) = 2.M_{0B}.CBF.t.e^{-t/T_{1B}}.q \tag{7.2}$$

Additionally, if the transit delay is taken into account, the time width of the bolus that passed the imaging slice will be t-$\delta$t before complete bolus passage. Then Eq.7.2 can be written as [36];

$$\Delta M(t) = \begin{cases} 0 & \text{t}<\delta\text{t} \\ 2.M_{0B}.CBF.(t-\delta t)e^{-t/T_{1B}}.q & \delta\text{t}<\text{t}<\delta\text{t}+\tau \\ 2.M_{0B}.CBF.\tau.e^{-t/T_{1B}}.q & \delta\text{t}+\tau<\text{t} \end{cases} \tag{7.3}$$

Eq.7.3 is named as standard model for perfusion quantification using ASL[11] . Formal derivation of Eq.7.3 is given in Appendix C.

However, the unknown parameters $\delta$t and $\tau$ take place in the equation beside the perfusion (CBF). In order to quantify perfusion, these terms must be eliminated or determined correctly. Additionally, simultaneous determination of CBF with $\delta$t or $\tau$ necessitates more than one measurements, which doubles the scan time and be a

[11] In some papers, $\alpha$ takes place as a multiplicative factor in the equations 7.2 and 7.3. It is named inversion efficiency and equal to 0.5 for saturation pulse, and 1 for perfect inversion pulse. This factor can also be lumped into q.

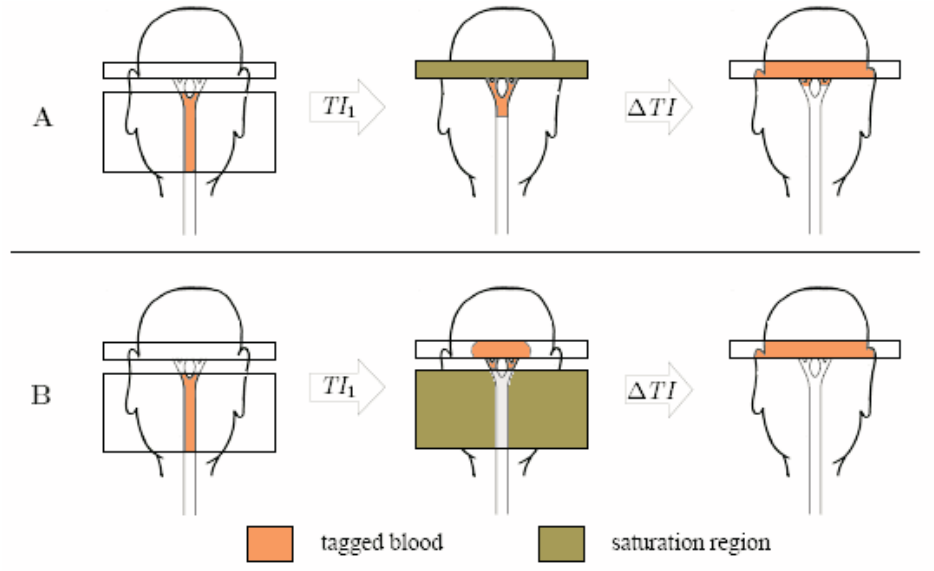


**Figure 7.4** QUIPSS sequence uses an extra saturation pulse applied at time $TI_1$. At $TI_2$ the image is acquired by imaging pulse. A)QUIPSSI B)QUIPSSII sequences [9].

disadvantage for the method.

**7.1.3.1 QUIPSS I.** QUIPSS (Quantitative Imaging of Perfusion Using a Single Subtraction) is a module that can be used with PASL sequences. This module consists of an additional saturation pulse applied in both the tag and control experiments [36].

When the additional saturation pulse applied to the imaging pulse at time $TI_1$, the contribution of the blood to the difference signal up to $TI_1$ is removed. Then, imaging pulse is applied at $TI_2$ (Figure 7.4). As a result, time width of the contributing bolus will be $\Delta$TI, and the magnetization difference can be written as;

$$\Delta M = 2.M_{0B}.CBF.\Delta TI.e^{-TI_2/T_{1B}}.q \tag{7.4}$$

where $\Delta$TI is a scan parameter which is equal to $TI_2$-$TI_1$ (in the literature TI is sometimes used as the synonym of $\Delta$TI). Because of the disturbance of the flowing spins on the imaging plane by saturation pulse, QUIPSS I is not amenable to multislice imaging.

**7.1.3.2 QUIPSS II.** The saturation pulse is applied to the inversion volume at time $TI_1$ (Figure 7.4). In this case, only the blood leaving the inversion volume up to $TI_1$ will have chance to contribute to the magnetization difference. If the conditions,

$$\begin{aligned} TI_1 &< \tau \\ TI_2 &> TI_1 + \delta t \end{aligned} \tag{7.5}$$

is hold, then the width of the contributing bolus is determined. The magnetization difference can be written as;

$$\Delta M = 2.M_{0B}.CBF.TI_1.e^{-TI_2/T_{1B}}.q \tag{7.6}$$

QUIPPS2 is more advantageous than QUIPPS1 because, it is amenable to multislice imaging.

**7.1.3.3 Q2TIPS.** This is a modification of QUIPPS II, where the saturation pulse is replaced by train of pulses applied thinner sections at the proximal part of inversion volume (Figure 7.5). This is done for sharper slice profiles.

New scan parameters are introduced with this sequence [10], the key aspect is to set the parameters as the cut-off velocity will be larger than the velocity of blood in the saturation volume. In the further parts of the thesis, Q2TIPS will be used for measurement of perfusion.

## 7.2 Assessment of Perfusion Parameters from ASL Measurements

As seen in previous sections, ASL imaging is based on the difference images which are the maps of difference of magnetization measured in control and tag experiments for each pixel. But, the difference magnetization used for perfusion quantification is on the order of 1% of static tissue magnetizations [9]. So, the measurements are

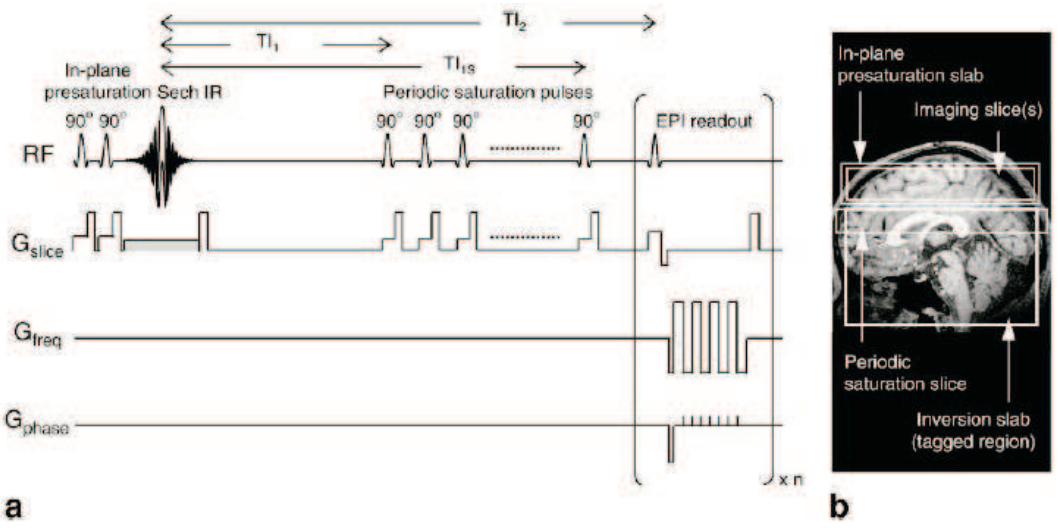


**Figure 7.5** Q2TIPS Sequence. The extra saturation pulse of QUIPSS2 is replaced by thin periodic saturation pulses which provide better slice profiles [10].

repeated several times (e.g 50 tag + 50 control images).

For perfusion measurements, QUIPSS2 or Q2TIPS is used to control the temporal width of the bolus and reduce the transit delay sensitivity of the perfusion calculations. There is a standardized use of 10-cm long inversion plane with 1-cm gap from the imaging volume. The first length produces inverted bolus of spins with nearly 700 ms temporal width, whereas the latter results in transit delay of 400-1200 ms in a single slice [36].

Without using QUIPSS2, one has to quantify CBF by using Eq.7.3. However, it is essential to simultaneously determine other parameters accurately appearing in Eq.7.3. This increases the scan time as stated previously.

However, by using QUIPSS2 these parameters disappear as in the Eq.7.6 but one must have an approximate guess about these parameters in order to satisfy the conditions stated in Eq.7.5.

When the parameters $TI_1$ and $TI_2$ fall out of the range stated in Eq.7.5, then

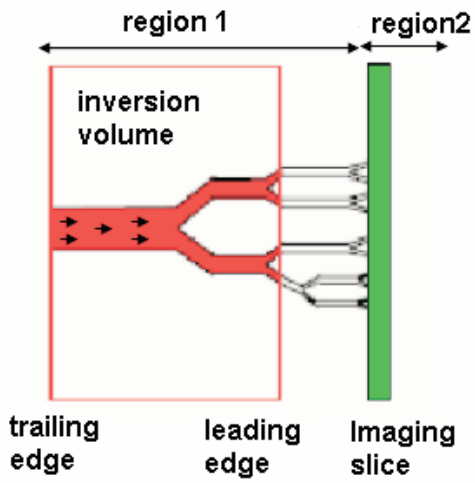


**Figure 7.6** Eq.7.7 describe ΔM in four phases, with respect to the positions of the leading edge (front side) and trailing edge (backside) of the inverted spins. They are in region 1 if they didn't arrive to the imaging slice, otherwise they are accepted to be in the region 2.

the measured magnetization difference can be written in four phases as,

$$\Delta M = \begin{cases} 0 & \mathrm{t}<\mathrm{TI}_2 \\ 2.M_{0B}.CBF.(TI_2-\delta t)e^{-t/T_{1B}}.q & \delta\mathrm{t}<\mathrm{TI}_2<\delta\mathrm{t}+\tau \\ 2.M_{0B}.CBF.TI_1.e^{-t/T_{1B}}.q & \mathrm{TI}_1<\tau \text{ and } \delta\mathrm{t}+\tau<\mathrm{TI}_2 \\ 2.M_{0B}.CBF.\tau.e^{-t/T_{1B}}.q & \mathrm{TI}_1>\tau \text{ and } \delta\mathrm{t}+\tau<\mathrm{TI}_2 \end{cases} \tag{7.7}$$

in terms of QUIPPS2 and Q2TIPS parameters, including all possible conditions [37].

If both the leading and trailing edge are in region 1, then ΔM is 0 which is described as in phase-1 of Eq.7.7. If leading edge is in region 2 and trailing edge is in region 1, then ΔM is calculated as described in phase-2 of equation. If both the leading and trailing edge are in region 2 and the saturation is successful (saturation pulse applied before all the inverted bolus passes through the saturation plane) then ΔM is calculated as described in phase-3 of equation. If both the leading and trailing edge are in region 2 but the saturation is not successful (saturation pulse applied after all the inverted bolus passes through the saturation plane) then ΔM is calculated as described in phase-4 of the same equation.

A compact form of Eq.7.7 can be written as,

$$\Delta M = 2.M_{0B}.CBF[min(\delta t - \Delta TI, 0) - (\delta t - TI_2)].e^{-TI_2/T_{1B}}.q \qquad (7.8)$$

Such an equation is defined by Wang et al. in [38] and used in [39] for quantification of CBF. For quantification of CBF, both Eq.7.6 or Eq.7.7 can be used. The choice depends on the experimenter or the clinician.

In the next two sections, these distinct methods will be investigated.

**7.2.0.4 Single-Subtraction Method.** If Eq.7.6 is used, tag and control images are taken with single set of scan parameters. The resulting images were subtracted and used in Eq.7.6. This method is also named as single-subtraction method.

In this method, the scanning strategy is as following:

- Set $TI_1$ such that it will be smaller that $\tau$ (e.g 700 ms). But, while satisfying this condition, setting $TI_1$ as large as possible, is advantageous for SNR considerations.
- Set $TI_2$ such that it will be larger that $TI_1+\delta t$ (e.g 1400 ms). But, while satisfying this condition, setting $TI_2$ as small as possible, is advantageous for SNR considerations.

After the scanning, by subtracting the tag image from control image, $\Delta$M's are obtained for every pixel. Then Eq.7.6 is used for every pixel to obtain perfusion (CBF) maps. $TI_1$ and $TI_2$ in the equation are scan parameters and set by the user, $T_{1B}$ ($T_1$ of blood) is a assumed value from the literature [10, 40], $M_{0B}$ (equilibrium magnetization of blood) is calculated as described in Appendix D, lastly q is assumed (usually between 0.85-1) [36, 41, 42] or approximately calculated[12] [10]. Using all these parameters with

[12] If $T_1$=900ms, $T_{1B}$=1300ms, $\tau+\delta$=1000ms, f=0.01s$^{-1}$, t=1400ms and $\lambda$=0.9, then q is approximately 0.93.

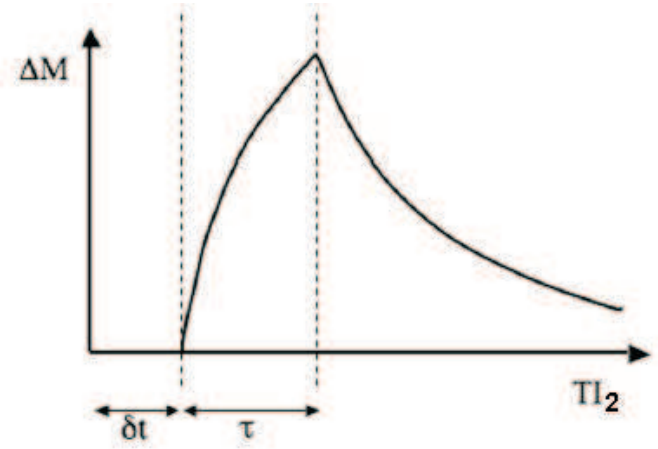


**Figure 7.7** Kinetic curve, which shows the change of magnetization difference in time can be seen in the figure. Time parameters $\delta$t and $\tau$ are represented in the curve as shown [11].

Eq.7.6, CBF can be calculated.

**7.2.0.5 Multiple-Subtraction Method.** If Eq.7.7 is used, tag and control images are taken with multiple set of scan parameters. The resulting images were subtracted and used in Eq.7.7 for simultaneous quantification of both CBF and $\delta$t. This method is named as multiple-subtraction method. This method is advantageous over singe-subtraction method, especially in the cases of cerebrovascular diseases. In normal human brain, both $\delta$t and $\tau$ can be approximately guessed, but for example in the case of occlusive diseases, $\delta$t can be increased for the pixels in region of interest (ROI) resulting in inaccurate quantification of perfusion for that pixels if single-subtraction method is used. So, in some clinical cases, the absence of a priori knowledge of the vascular structure makes the perfusion parameters $\delta$t an $\tau$ unpredictable, so these parameters must be determined simultaneously with CBF for accurate quantification.

In order to do that, the magnetization difference of the pixels in the imaging slice is sampled along a number of time-points (Figure 7.7). Then Eq.7.7 is fitted to the obtained points, where the results of the fitting process gives the quantified values of perfusion parameters.

If multi-subtraction is used without the QUIPSS2 or Q2TIPS module, the fit-

ting procedure will result in determining three parameters ($\delta$t, $\tau$ and CBF). For that, sampling must be performed in at least three time points.

If multi-subtraction is used with the QUIPSS2 or Q2TIPS module, the fitting procedure will result in determining two parameters ($\delta$t and CBF), because $\tau$ is equal to the scan parameter, $TI_1$. But this holds for the case of successful saturation of the flowing spins at $TI_1$. So, one must be sure that the applied $TI_1$ is smaller than the time interval that trailing edge of the inverted bolus will cross the 10 cm distance. There is no problem of using the $TI_1$ as for the normal brain in pathological cases. Because blood slows down in those cases, the natural temporal width of inverted flowing spins is automatically larger than the normal cases, so successful saturation is guaranteed.

# 8. Results and Discussion

The technical background of AS and DSC perfusion imaging were given in the previous parts of this thesis.

In this chapter, the results obtained using these methods will be presented and discussed. For this purpose, images taken from two healthy volunteers and two patients will be used. ASL patient scans were performed as addition to a routine DSC-containing clinical procedure. Both the patient and volunteer scans were performed in Acibadem Hospital using 3T Siemens Trio MR device.

Volunteer scans consist of anatomical scans, inversion recovery echo planar imaging (IR-EPI) scans and ASL scan with single parameter. Patient scans consist of anatomical scans, DSC scan, IR-EPI scans and ASL scans with multi parameter strategy.

Segmentation data (IR-EPI) is used together with the ASL data during quantification of ASL, this means that both scans must have the same voxel size and distortion effects. So; field of view (FOV), matrix size and bandwidth of two sequences were set equal.

Among all four subjects, volunteer-1 scanned with different parameters with 260 mm. FOV and 64×64 matrix resulting in 4 mm in-plane resolution. Other three subjects were scanned with 295 mm FOV and 128×128 matrix resulting in 2.3×2.3 mm in-plane resolution.

The following sections of the thesis start with the description of the imaging protocol, but mainly focuses on the presentation of the results. They are organized on the imaging techniques and post-processing methods. Measurement results and the parameter maps are given at the end of the chapter.

## 8.1 DSC Results

Hemodynamic parameters (CBV and CBF) provide information about the malignancy and degree of the tumor. Patient-1 suffers from glial sarcoma, had radiotheraphy, chemotheraphy and a brain operation before this scan. The decreased perfusion is measured in the related sites, which is a sign of necrosis or inactivity of the cells (Figures 8.2, 8.14). Patient-2 suffers from a high grade heterogenous tumor and hydrocephaly. Increased perfusion was measured in the neighborhood of the cystic part in the perfusion images. Increased volume of CSF is observed in hydrocephaly patients. The volumes with CSF is not perfused, so decreased areas of perfusion can be seen in perfusion maps (Figures 8.3, 8.15). These patients were subject to both DSC and ASL methods for perfusion measurements. In this section, the DSC protocol will be described and the results will be presented.

DSC-MR gradient echo EPI images were collected during the pass of a bolus after the injection of the tracer with power injector at a rate of 5 ml/s immediately followed by the bolus injection of the saline (total of 20 ml at 5ml/s rate). First 10 of the total 50 images acquired before the injection were used to determine the baseline signal. Other parameters were, TR/TE: 1360/31 ms, BW = 1500 Hz/pixel, 128 x 128 matrix over a 24x24 cm FOV covering the whole brain in 5 mm thick 19 slices.

DSC-MR images were converted to the concentration time courses assuming that transverse relaxation change due to exogenous tracer is linearly dependent on the tracer concentration. After the application of a 3x3 uniform smoothing kernel to the raw image data, singular value decomposition (SVD) decomposition were applied with threshold value of 0.15.

Arterial input function were selected by visual inspection from the sites of Internal Carotid Artery (ICA) and peripheral branches of Middle Cerebral Artery (MCA) taking into account the rapid tracer arrival and the small FWHM of the candidate voxels. As a result CBF, CBV and MTT maps are obtained

### 8.1.1 Patient-1

Perfusion parameter maps of patient-1 are given in figure 8.2.

### 8.1.2 Patient-2

The perfusion parameter maps of patient-2 is obtained by using identical procedure of patient-1's and can be seen in figure 8.3.

## 8.2 Segmentation

In the related chapter it is stated that brain consists of three basic kind of tissues; gray matter (GM), white matter (WM) and cerebrospinal fluid (CSF).

Segmentation means distinguishing these tissue types. For the proposed works in the thesis, segmentation is necessary for two reasons. Firstly, for absolute quantification of CBF, the parameter $M_{0B}$ appearing in Eq. 7.6 must be correctly determined. For determination of $M_{0B}$, one must find the $M_0$ of WM as described in Appendix D, so it necessitates the segmentation of WM.

Secondly, handling the mean perfusion values for WM and GM may be useful for multi modality comparisons, testing the validity of the method and for clinical cases.

In MRI, for distinguishing the tissue types, measurable tissue specific parameters are usually used, these are $T_1$, $T_2$, spin density $\rho$. As stated before, the magnetization is directly measured in MRI. Tissue specific parameters are determined by using multiple scans results obtained with appropriate scan parameters.

In this thesis work, segmentation will be based on the $T_1$ of the tissue. To find tissue $T_1$, magnetization is sampled during the longitudinal relaxation. For that pur-

pose, IR-EPI sequence is used. Sequence starts with $\pi$ pulse, thus the spins systems behaves as inversion recovery relaxation and after delay time (TI) later a $\frac{\pi}{2}$ pulse is applied, which is also named as imaging pulse, because it flips the recovering magnetization onto transverse plane and samples the net magnetization at the time it is applied.

IR-EPI with two varying TI's (250, 3500 ms) is used to create T1 maps which are used for segmentation. Delay time (TR-TI) was kept constant (15s) during these scans. TI values was selected by taking into account the fastest and slowest T1 recovered brain tissue (WM and CSF) in order to be confident about the polarity of the net magnetization. A single shot, gradient echo EPI images with TR=20s is applied to measure equilibrium magnetization. It is assumed that the net magnetization at t=0 is bounded with M0$\pm$0.05M0. So, this measurements used twice in the recovery sample of the spin system, once just after the $\pi$ pulse (in the beginning of relaxation) and lastly on the relaxed time domain. The sampled magnetizations at four time-points were fitted to the Eq.5.9 using Levenberg-Marquardt algorithm with nonlinear least squares method. As a result, both $T_1$ and $M_0$ maps were obtained for each voxel.

$T_1$ of WM and GM are determined by using histograms of $T_1$ maps which are generated by using 3000 bins, where each bin is averaged with 21 consecutive bins. The resultant histogram was fitted to the sum of three Gaussian functions, the centres of each gaussian is equal $T_1$ of WM, GM and CSF [43]. If the slice lacks CSF, then the histogram is fitted to the sum of two gaussians. Then, masks for WM, GM and CSF is obtained by applying thresholds to the image determined from the histogram by visual inspection.

### 8.2.1 Volunteer-1

As described above, first the $T_1$ and $M_0$ maps were obtained using fitting procedure described in the earlier section(Figure8.4).

The histogram of $T_1$ map of one selected slice is fitted to the sum of two gaussian functions. The centres of the gaussians are equal to the $T_1$ of WM and GM. $T_{1WM}$ is found as 0.783 s. and $T_{1GM}$ is found as 1.295 s. The voxels with value between 0.5 and 0.9 in $T_1$ map is accepted as WM voxels, similarly the voxels within 1.1 and 1.7 is accepted as GM voxels. So the masks for GM and WM can be produced (Figure 8.5.c).

### 8.2.2 Volunteer-2

The segmentation procedure is the same as the volunteer-1's. So, only the results will be presented graphically (Figure 8.6).

### 8.2.3 Patient-1

$T_1$ maps are obtained as described in the previous sections. However, as seen in figure 8.7.b, the voxels in the site of necrosis has very close $T_1$'s to the $T_1$ of GM. So, in order to prevent miscalculation of the mean $T_1$ of GM, the histograms of the half-image containing the contralateral of the site of necrosis are used to estimate the mean $T_1$'s.

### 8.2.4 Patient-2

The segmentation procedure is the same as the patient-1's. So, only the results will be presented graphically (Figure 8.8).

## 8.3 ASL Results

For ASL measurements, a pulsed ASL sequence was thin slice periodic saturation (Q2TIPS) with PICORE tagging is used. A gradient echo EPI was used to acquire five slices, inferior to superior with slice thickness = 8 mm, TE = 23 ms, TR = 2500 ms, PASL gap = 10 mm, GRAPPA (x2) used with maximum number of reference lines.

For volunteer scans, single-subtraction strategy is used with TI1 = 600 ms. and TI2 = 1450 ms. 60 control-tag pairs were acquired for quantification of CBF by using Eq. 7.6 where q is assumed to be 0.85.

For patient scans, multiple-subtraction strategy is used with with TI1 = 600ms and varying TI2 = 800, 1000, 1400 ms (it means three delay times TI with 200, 400, 800 ms), transit delay and CBF were quantified simultaneously by pixel-by-pixel fitting the difference signal series to the Eq. 7.8 using a nonlinear least squares fitting method. For each measurement, 40 images (control-tag pairs) were acquired.

Other works that use multiple-subtraction strategy may employ different TI's and NEX's [44, 45, 11]. Optimal design of TI's and NEX's is an active area of research [46], which tries to improve the accuracy of quantification while reducing the scan time needed.

### 8.3.1 Volunteer-1

The equilibrium magnetization of blood ($M_B$) must be found for quantification of CBF. However, it is not possible to distinguish a voxel which is only filled by blood, because of the relatively low resolution of the EPI images.

Instead, from the voxels with containing only WM, $M_{WM}$ is calculated. This could be done by using any of the three methods described in Appendix D. For volunteer-1, the arithmetical mean of all masked pixels was 1233.8, the perfect pixel

with the $T_1$ closest to the $T_{1WM}$ had $M_0$ equal to 1014.7, whereas the gaussian method gave 1142.5 (Figure 8.1). To decrease the weight of possible mis-segmented pixels on the calculation of $M_{WM}$, we prefer the gaussian method which seems to provide better results.

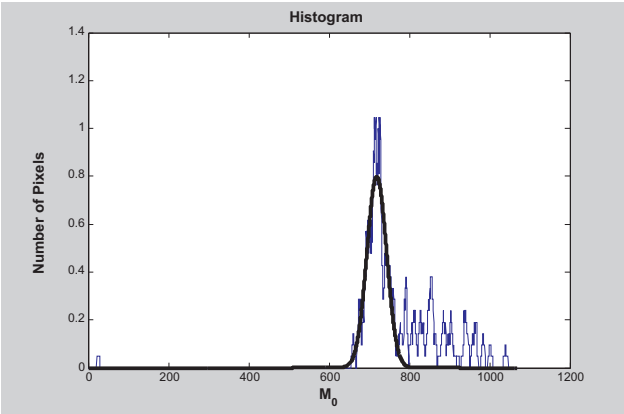


**Figure 8.1** Histogram of $M_0$ of WM pixels. The equilibrium magnetization is equal to the centre of gaussian function.

Then, $M_B$ is calculated by using Eq.D.1. $T^*_{2WM}$ and $T^*_{2B}$ is assumed to be 40 and 100 ms [10].

After calculating $M_B$, the $\Delta M$ maps obtained from measurements are used for the quantification of CBF. Both the $\Delta M$ and CBF maps is presented in figure 8.9.

The mean perfusion values of GM and WM is used for the validation of the method. Perfusion maps including only WM or GM pixels were presented in the given figures. By using these maps, calculation of mean perfusion value may be performed in various ways (the following comparison is similiar to the calculation of $M_{WM}$).

One could find the average of all pixels presented for tissue specific CBF maps. As an alternative method, we can use the histogram of these maps. If these histograms are fitted to a gaussian function, the mean CBF value is determined from the mean of fitted gaussian.

The latter method may provide better results for determination of mean perfu-

sion values. Because, arteries are presented as a bright spot in most of the perfusion maps, and they are mostly segmented as GM as a result of partial volume effect. Thus, using the former method would result in overestimation of mean values, whereas the latter method reduces the weights of these extreme voxels (Figure 8.10 and 8.11).

### 8.3.2 Volunteer-2

The procedure is the same as the volunteer-1's. So, only the results will be presented (Figure 8.12 and 8.13).

### 8.3.3 Patient-1

CBF and transit time maps are obtained simultaneously using multiple-subtraction approach. The results are presented in Figure 8.14.

### 8.3.4 Patient-2

The procedure is the same as patient-1's. The results are presented in Figure 8.15.

## 8.4 Comparison

In table 8.1, the mean WM and GM perfusion values of four subject measured by ASL, are displayed. As described in the previous section, among the two methods, Gaussian fitting is expected to provide more accurate mean values than the simple mean, because it is capable of excluding the bright points that are seen in parameter maps.

**Table 8.1**
Mean perfusion values of GM and WM in all acquired slices is calculated by two methods in ASL. Calculations were performed for all four subjects.

| Tissue CBF | Simple Averaging | | Gaussian Method | |
|---|---|---|---|---|
| | WM | GM | WM | GM |
| Volunteer-1 | 12.9±8.8 | 40.2±18.1 | 7.1±4.1 | 36.6±4.7 |
| Volunteer-2 | 28.6±25.2 | 49.7±27.1 | 18.2±4.3 | 46.5±8.5 |
| Patient-1 | 20.4±12.6 | 64.6±40.1 | 18±3.9 | 60.3±7.2 |
| Patient-2 | 12.2±7.6 | 87.9±40.1 | 10.9±3.1 | 63.1±8.4 |
| Average | 18.5±7.6 | 60.6±20.7 | 13.5±5.4 | 51.6±12.3 |

Mean values of GM and WM perfusion are reported as 65.3 and 21.4 in [47], 42.0 and 22.2 in [48] with the units ml/100g.1min. If compared with these reported PET measurements, the results obtained by ASL in this work can be found acceptable.

However, there are still some mechanisms which could be responsible for misquantification of perfusion in specific tissues. One is the partial volume effect; in volumes which is comparable with the voxel volume in ASL scans, more that one tissue types may be counted inside the voxel. This is not an issue for most of the WM voxels because of the homogenous distribution of this tissue type. But for GM pixels are distributed mostly in cortex rounded with the sagittal sinus and WM voxels. Thus, underestimation of perfusion can be observed in GM pixels.

If we examine Table 8.1 in detail, it seems that the Gaussian method gives less mean perfusion values. This can be due to decreased weight of arterial spots of perfusion maps in mean values.

An other error mechanism in perfusion measurements is the subject movement during scans. Because of the two volunteers are subject to long scans (only the scan with appropriate parameters is used for this results), the time interval between the acquisition of segmentation and perfusion data may result in increase of the segmen-

**Table 8.2**
Mean perfusion values of GM and pathologic volume obtained in ASL and DSC techniques. Calculations were performed for the patient subjects. Because of DSC provides relative quantitative values, all the measured perfusion values were normalized with respect to CBF of WM for comparison.

| | ASL | | DSC | |
|---|---|---|---|---|
| | $CBF_{GM}/CBF_{WM}$ | $CBF_{PAT}/CBF_{WM}$ | $CBF_{GM}/CBF_{WM}$ | $CBF_{PAT}/CBF_{WM}$ |
| Patient-1 | 3.35 | 0.91 | 4.86 | 0.81 |
| Patient-2 | 5.78 | 5.41 | 6.02 | 5.91 |
| Average | 4.56±1.71 | | 5.44±0.83 | |

tation errors. This can be recognized in figure 8.13, as the increase of WM perfusion in neighborhood of GM pixels. This also results in a decrease in the calculated mean of GM perfusion. This can be the possible mechanism to describe the reduced $CBF_{GM}/CBF_{WM}$ in ASL, if compared to the DSC data, which is presented in table 8.2.

In table 8.2, the normalized perfusion values of ASL and DSC are compared. Perfusion values are normalized (with respect to mean WM perfusion), because DSC methods provides only relatively quantitative results of CBF [13] . Perfusion in pathologic site ($CBF_{PAT}$) is measured by drawing ROI's using visual inspection, the mean value of CBF in ROI is calculated in terms of Gaussian averaging.

In Patient-1, $CBF_{PAT}$ is measured smaller than $CBF_{WM}$ in both the ASL and DSC methods. This reduced perfusion is the sign of necrosis. By looking the table 8.2, it can be seen that the $CBF_{PAT}$ of Patient-2 is smaller that $CBF_{GM}$. The ROI including the pathologic site consists some pixels with increased CBF, however simultaneously, mean decrease of perfusion in the site of pathology is the sign of heterogeneity of the

[13]However if a correction for tissue hematocrit is applied to DSC data, quantitative results can be obtained. Rempp et al. offered a global hematocrit correction factor [49] to overcome that problem. Hovewer, the constancy of that factor among all the tissues is assumed, which can introduce errors in absolute quantification.

**Table 8.3**
Parameters which are found during segmentation and quantification process. $T_1$'s of WM and GM are given in units of seconds, whereas the equilibrium magnetization of WM and blood are in artificial units.

| | $T_{1WM}$ | $T_{1GM}$ | $M_{0WM}$ | $M_{0B}$ |
|---|---|---|---|---|
| Volunteer-1 | 0.783 | 1.295 | 718.9 | 1142.5 |
| Volunteer-2 | 0.762 | 1.292 | 638.7 | 1015.1 |
| Patient-1 | 0.751 | 1.316 | 553.5 | 828.4 |
| Patient-2 | 0.729 | 1.351 | 592.6 | 886.9 |
| Average | 0.756±0.022 | 1.321±0.041 | 625.9±71 | 986.2±139.9 |

tumor in interest.

Lastly, table 8.3 shows the results of $T_{1WM}$, $T_{1GM}$, $M_{0WM}$ and $M_{0B}$ obtained from all the subjects.

For comparison with the literature, the results of two studies will be used:

- Stanisz et al. acquire $T_1$ relaxation time data acquired using an inversion recovery (IR) sequence with 35 TI values logarithmically spaced from 1 to 32,000 ms, 20s between each acquisition and the next inversion pulse (TR), and 2 averages. They reported the mean values and standard deviations of WM and GM $T_1$'s as 1084±45 and 1820±114 ms [40].

- Wansapura et al. perform $T_1$ measurements using a saturation recovery method with a variable TR spin-echo imaging sequence. They reported 832±10 and 1331±13 ms for WM and GM $T_1$'s [50].

Both of the studies were performed in 3T; among the two papers, the results obtained in this thesis work seems to agree with the results of Wansapura et al.

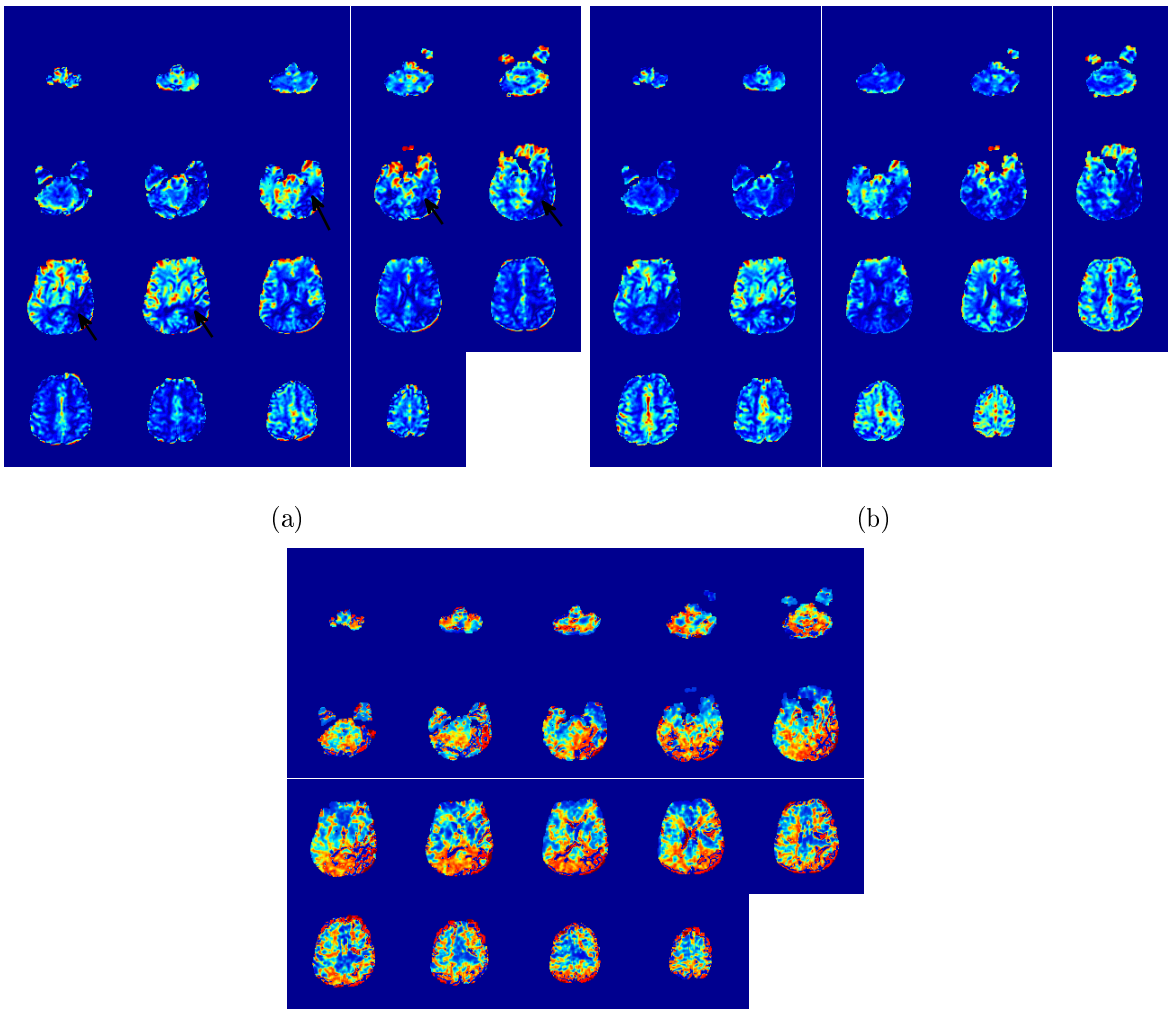

(a) (b)

(c)

**Figure 8.2** Perfusion maps of Patient-1. a) CBV map. The sites of necrosis are indicated by arrows, where decreased blood volume and blood flow is observed. b) CBF maps. c) MTT maps.

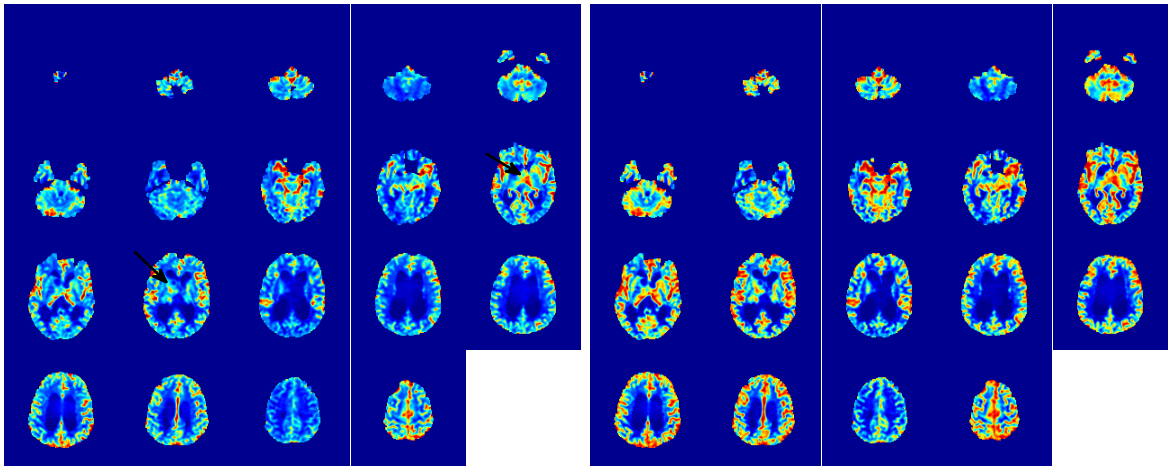

(a) (b)

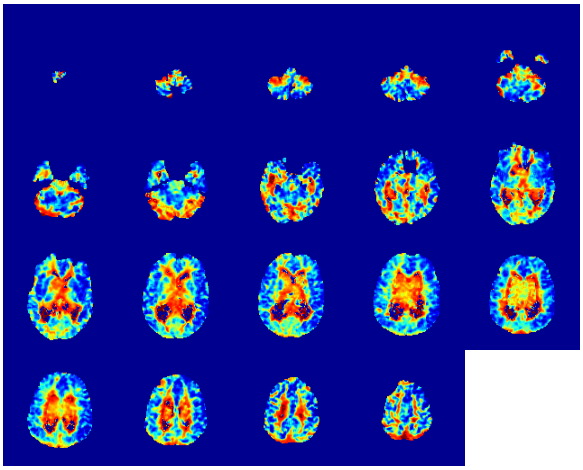

(c)

**Figure 8.3** Perfusion maps of Patient-2. a) CBV map. Increased perfusion areas are indicated in the neighborhood of the cystic part in the perfusion images. Decreased areas of perfusion can be seen in perfusion maps because of the increased volume of CSF. b) CBF maps. c) MTT maps.

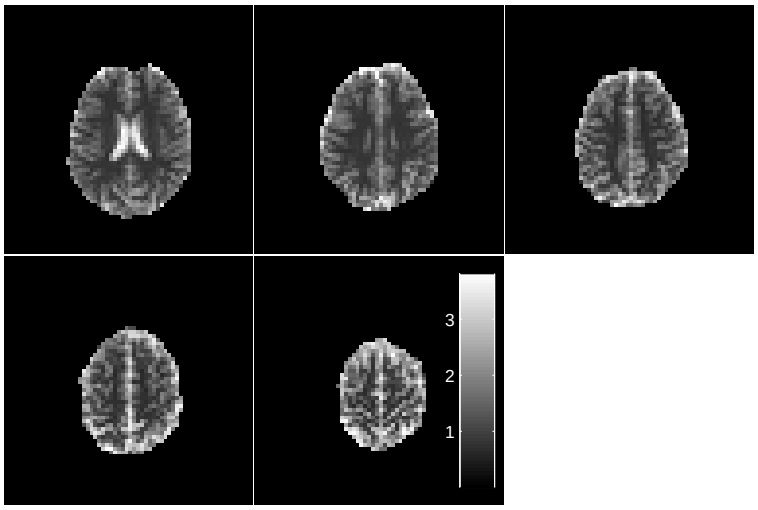


(a)

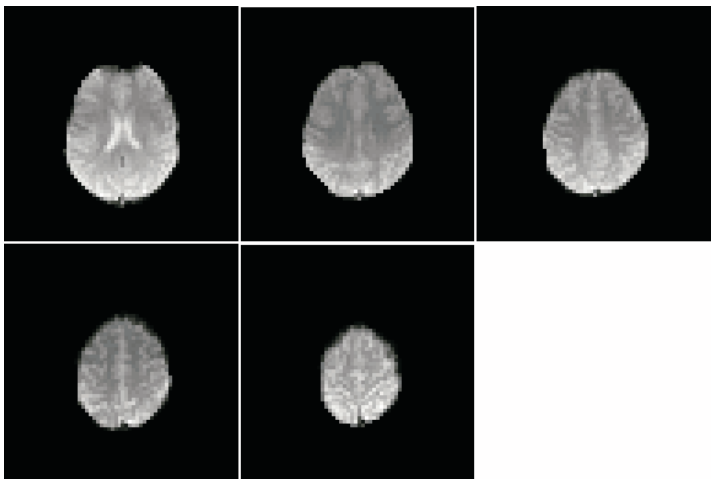

(b)

**Figure 8.4** (Data belongs to Volunteer-1) a) $T_1$ maps. The colorbar is shown in units of seconds. b) $T_2^*$ weighted equilibrium magnetization ($M_0$) maps

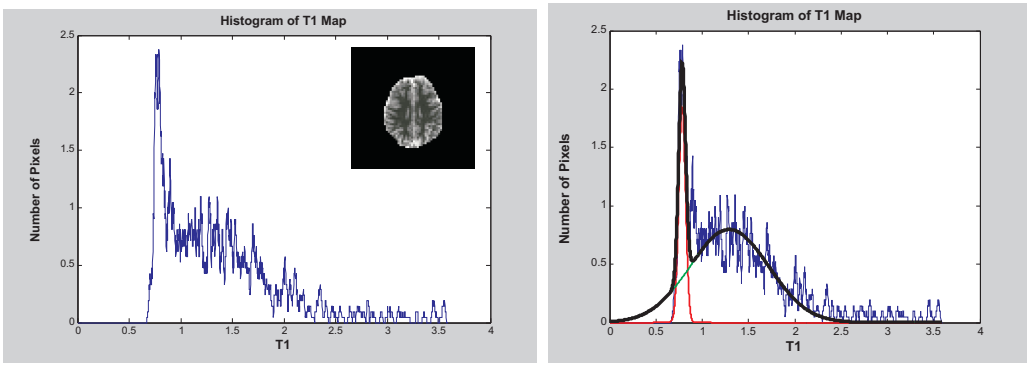


(a) (b)

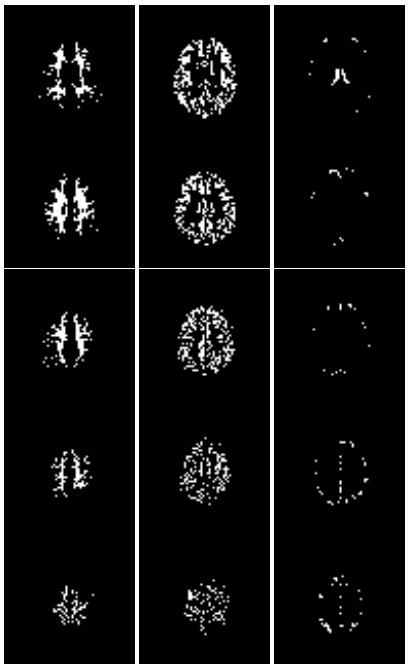

(c)

**Figure 8.5** (Data belongs to Volunteer-1) a) The histogram of a $T_1$ map of slice-2. b) The histogram of a $T_1$ map together with the fitted gaussian functions c) Masks of WM, GM and CSF tissues of five slices are given for the first, second and third columns.

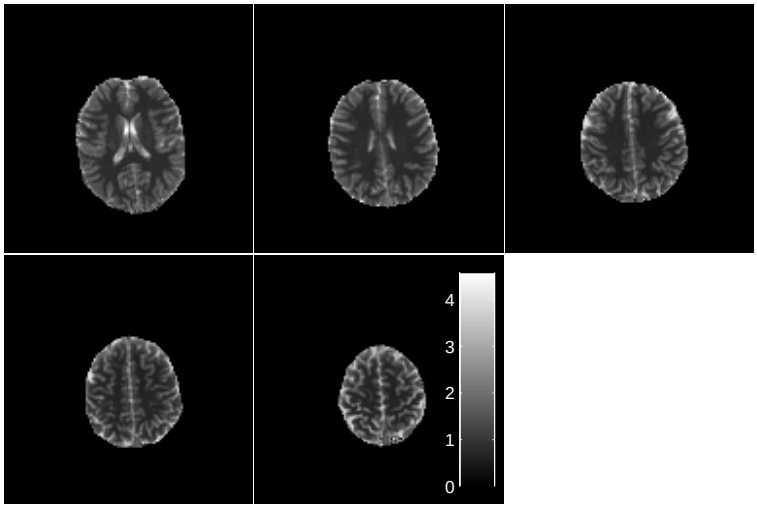


(a)

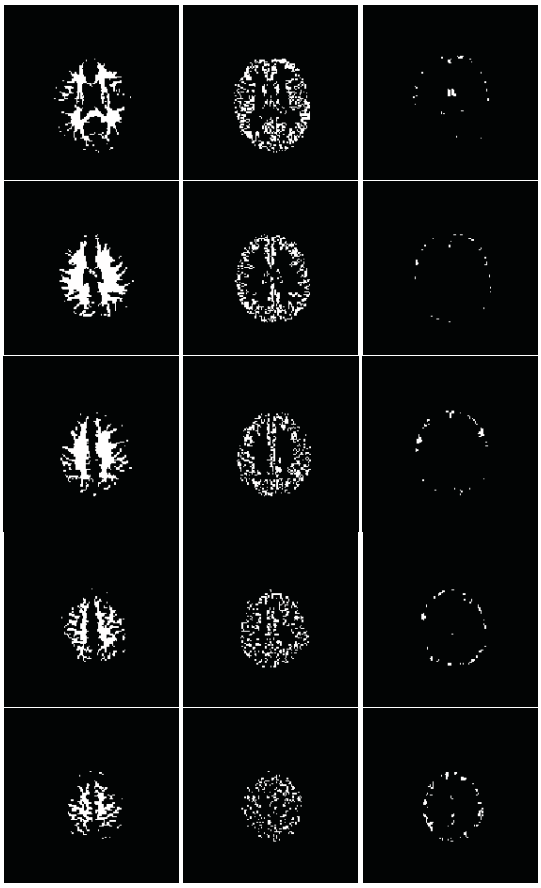

(b)

**Figure 8.6** (Data belongs to Volunteer-2) a) $T_1$ maps. The colorbar is shown in units of seconds. b) Masks of WM, GM and CSF tissues of five slices are given for the first, second and third columns.

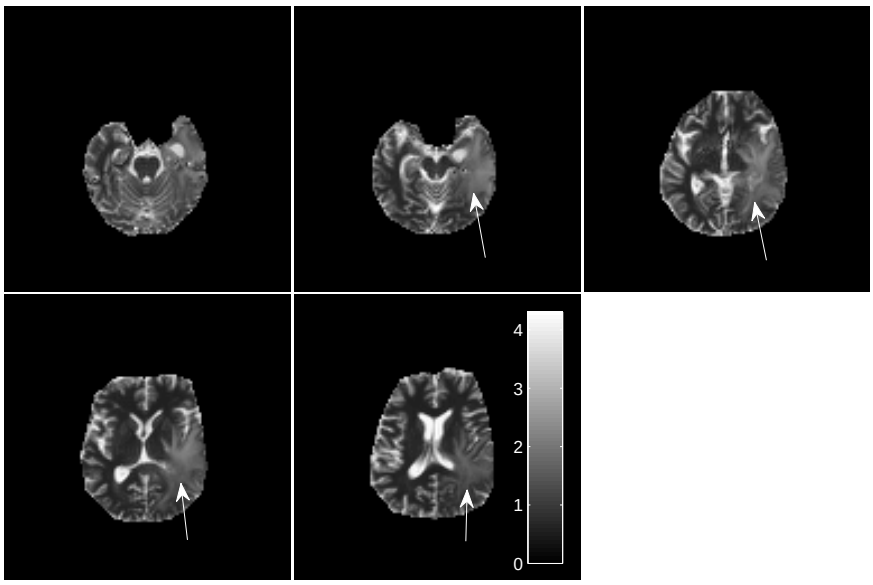


(a)

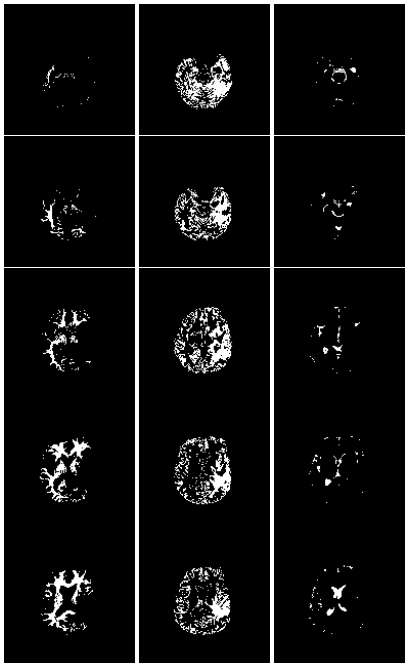

(b)

**Figure 8.7** (Data belongs to Patient-1) a) $T_1$ maps. The sites of necrosis are indicated by arrows. The colorbar is shown in units of seconds. b) Masks of WM, GM and CSF tissues of five slices are given for the first, second and third columns.

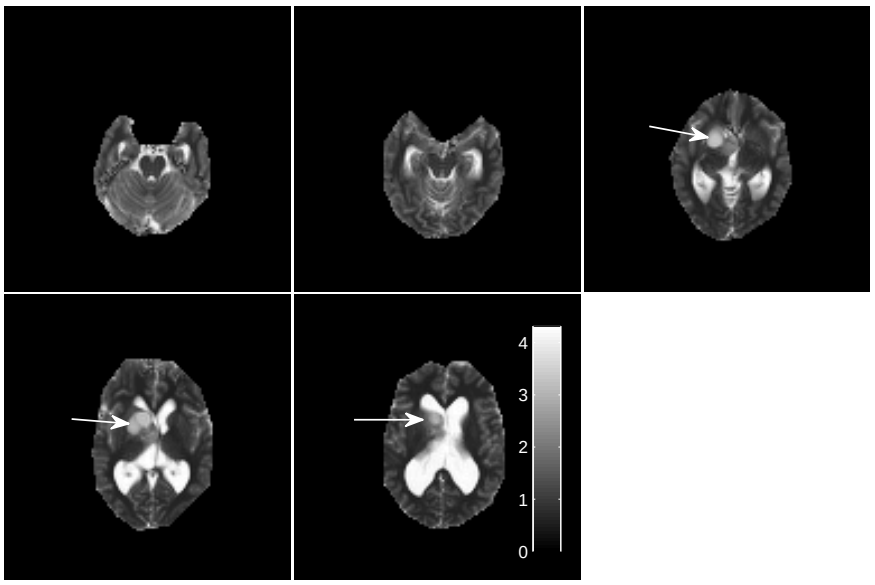


(a)

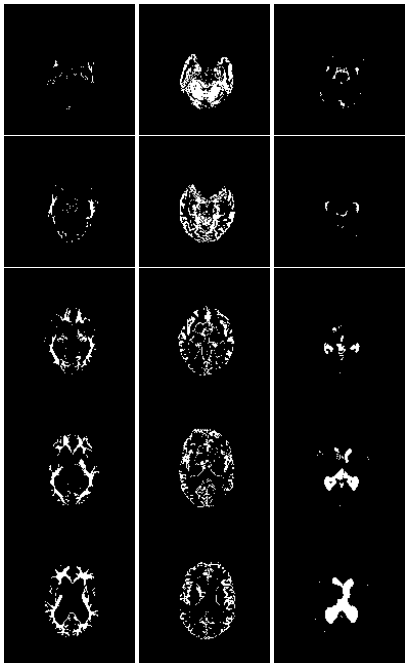

(b)

**Figure 8.8** (Data belongs to Patient-2) a) $T_1$ maps. The cystic part is indicated by arrows. The colorbar is shown in units of seconds. b) Masks of WM, GM and CSF tissues of five slices are given for the first, second and third columns.

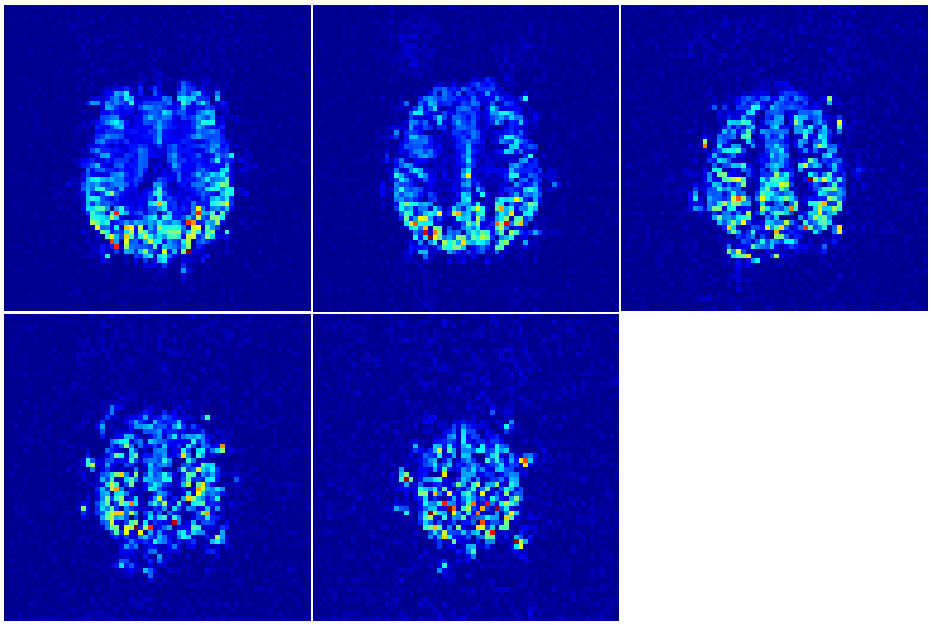

(a)

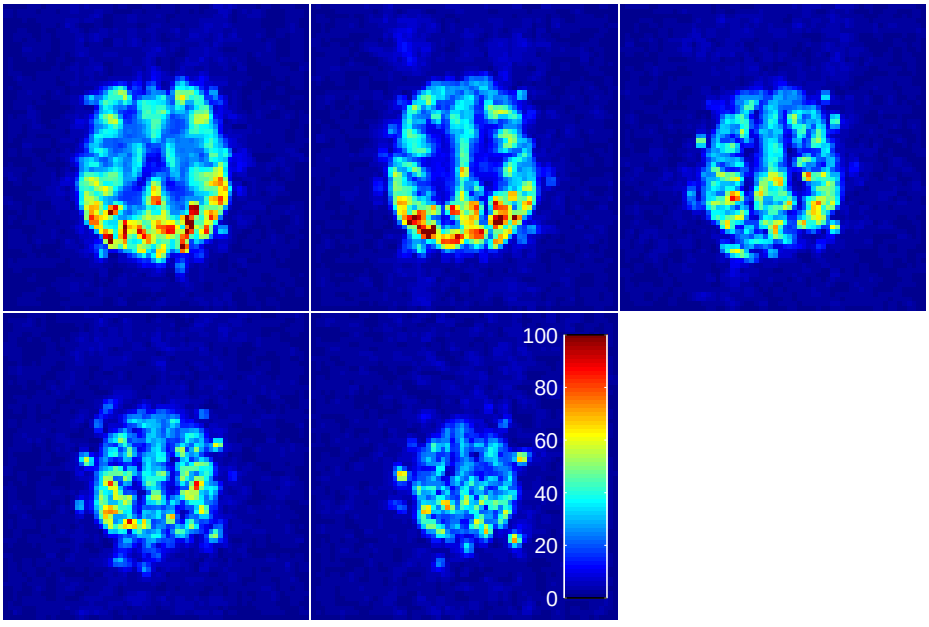


(b)

**Figure 8.9** (Data belongs to Volunteer-1) a) The magnetization difference map b) Quantitative CBF map with colorbar in units of ml/g.min.

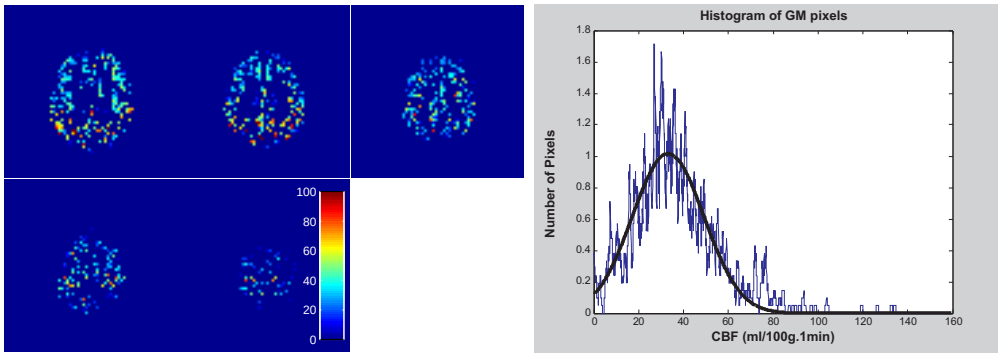


(a) (b)

**Figure 8.10** (Data belongs to Volunteer-1) a) The quantitative CBF maps of GM tissues. It is found by using the CBF maps and tissue masks. b) The histogram of GM pixels in the total five slices

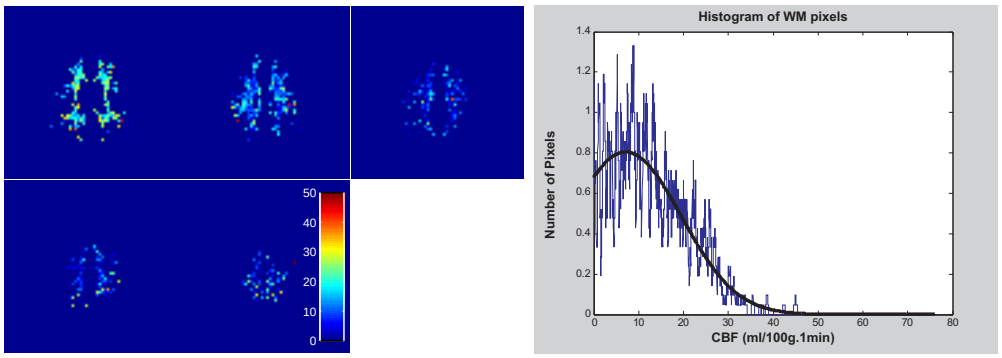


(a) (b)

**Figure 8.11** (Data belongs to Volunteer-1) a) The quantitative CBF maps of WM tissues. It is found by using the CBF maps and tissue masks. b) The histogram of GM pixels in the total five slices

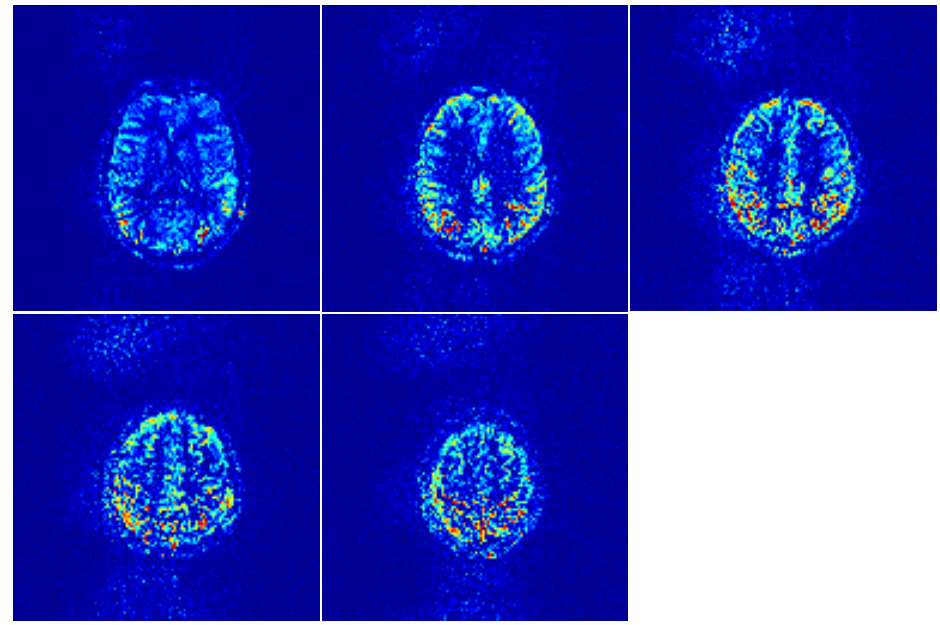

(a)

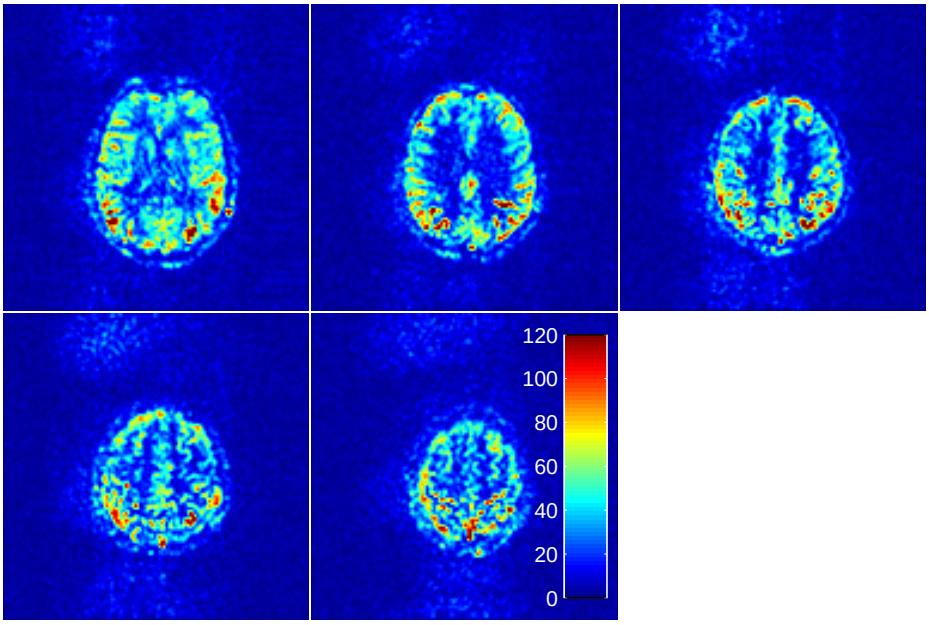


(b)

**Figure 8.12** (Data belongs to Volunteer-2) a) The magnetization difference map b) Quantitative CBF map with colorbar in units of ml/g.min.

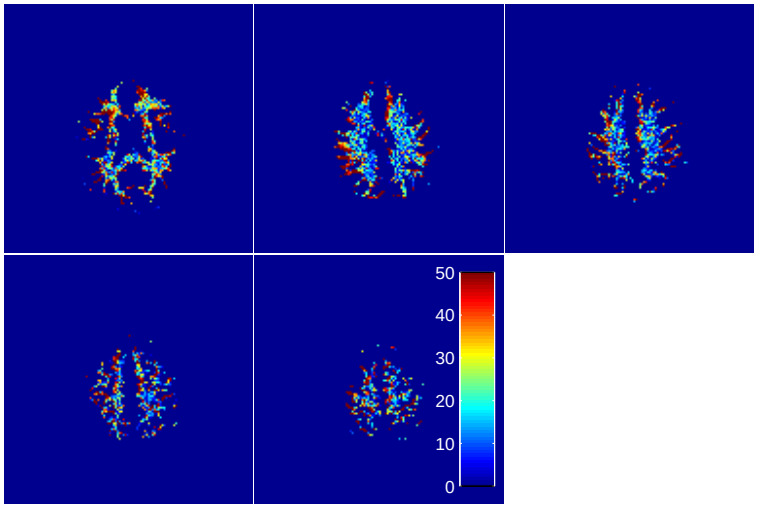


(a)

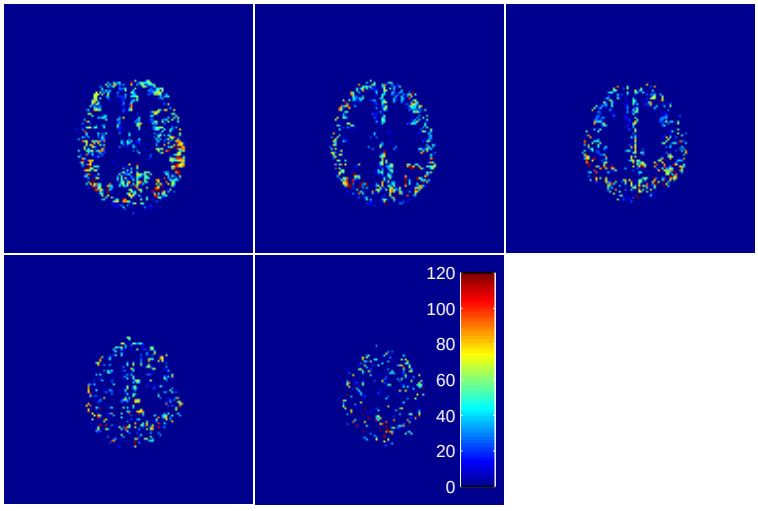


(b)

**Figure 8.13** (Data belongs to Volunteer-2) The quantitative CBF maps of a) WM and b) GM tissues

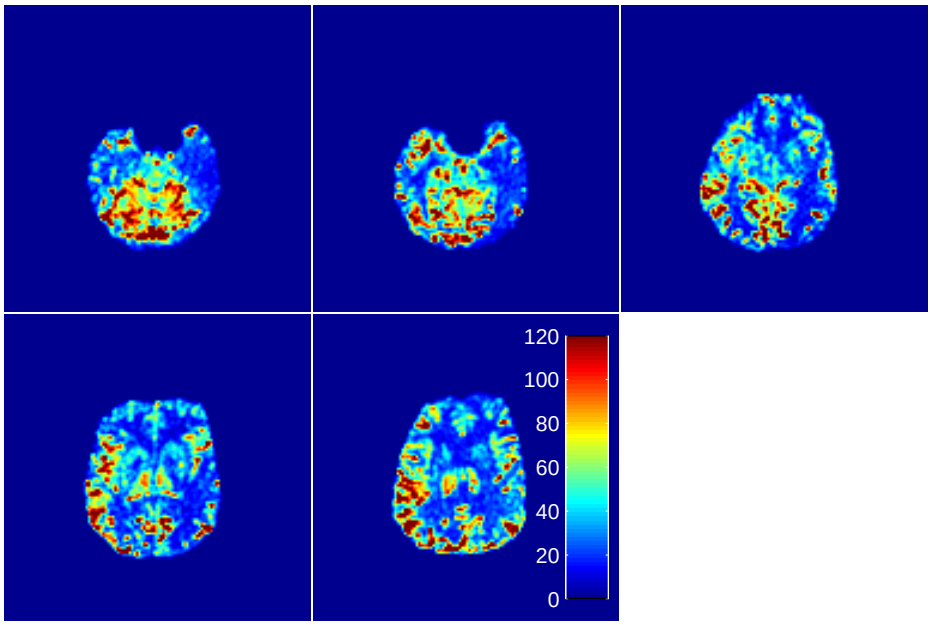


(a)

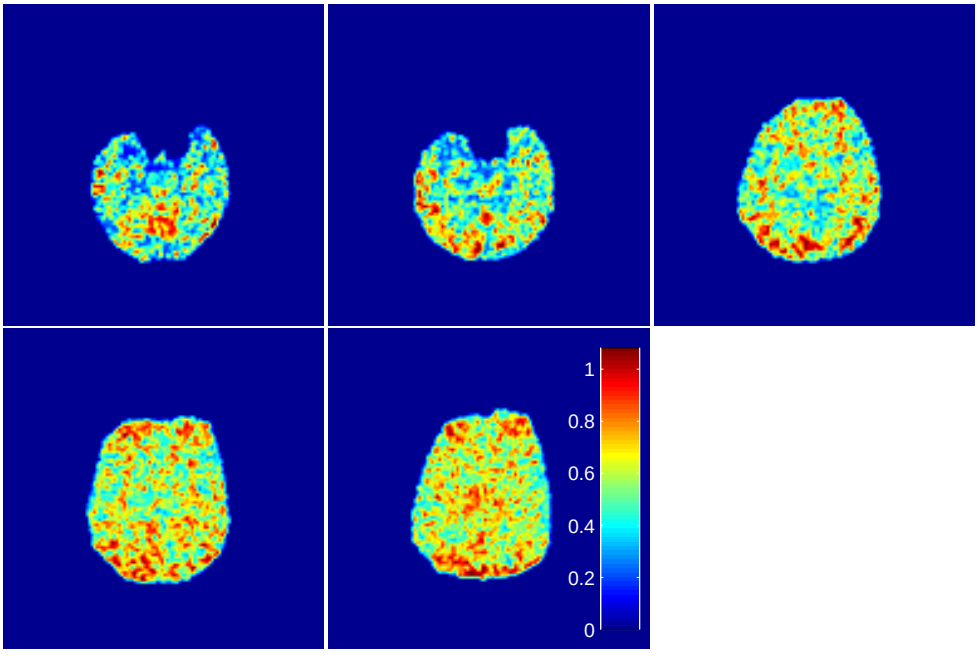


(b)

**Figure 8.14** (Data belongs to Patient-1) a) Quantitative CBF map with colorbar in units of ml/g.min. b) Transit time ($\delta$t) maps is shown with colorbar in units of seconds.

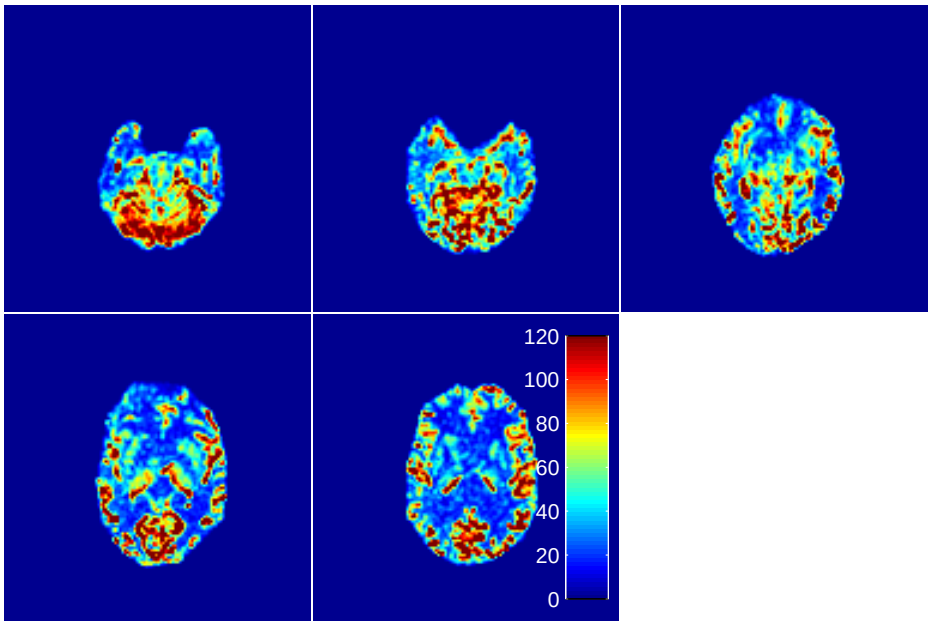


(a)

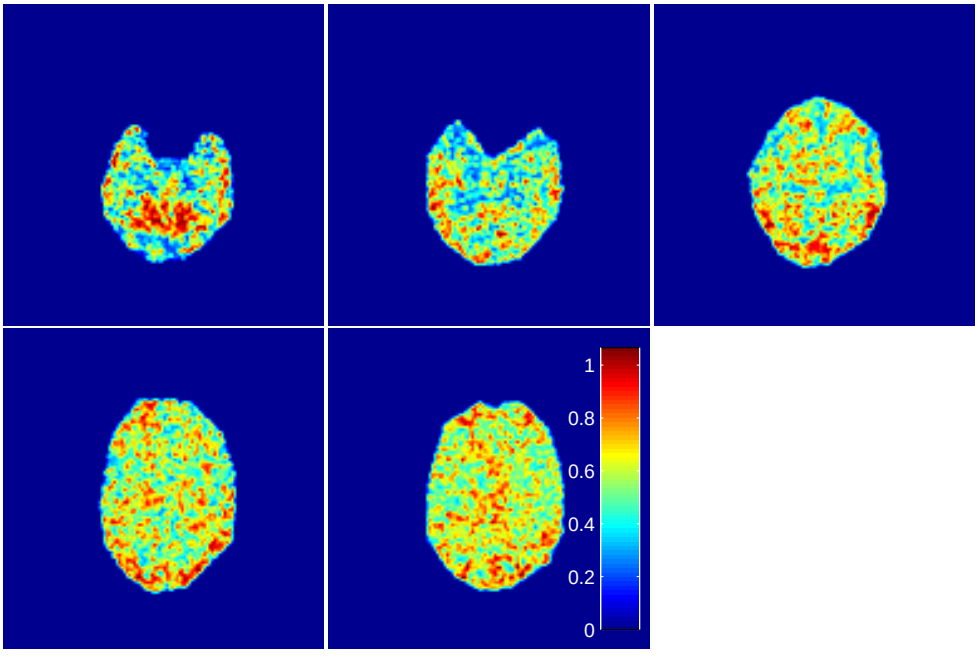


(b)

**Figure 8.15** (Data belongs to Patient-2) a) Quantitative CBF map with colorbar in units of ml/g.min. b) Transit time ($\delta$t) maps is shown with colorbar in units of seconds.

# 9. Conclusion and Future Works

In this work, brain perfusion measurements were performed in two normal volunteers and two patients with DSC and ASL methods using MRI scanner.

DSC is accepted to be a robust method for perfusion measurements. However, it is invasive in nature, i.e. it relies on the injection of an exogenous contrast agent. Additionally it provides only relatively quantitative (or semi-quantitative) results. But, contrast material enhances SNR of measurements, so perfusion parameter maps with high contrast can be obtained using this method without the need of temporal averaging etc. This reduces the time required for clinical scans.

ASL, as a result of this work is shown to be a candidate for robust measurement of perfusion noninvasively. The quantitative perfusion maps derived by ASL in this work gave acceptable mean values of perfusion for WM and GM when compared with the literature. But SNR is still low in ASL, even at 3T. So, measurements are repeated and the scan time is elevated. This can be a disadvantage in clinical usage.

In the future work, ASL studies may aim the optimum design of scan parameters, especially delay time (TI) and number of excitations (NEX). Besides decreasing the scan time, an optimum design may also provide better quantification of CBF and transit time ($\delta$t).

# APPENDIX A. MR Signal Change Due to Contrast Agent

When the bolus of contrast agent passes through the vasculature, the local magnetic properties change. The following part will focus on the measurement of tissue magnetization before and during the passage of the bolus, aiming to extract the local tissue properties from these measurements.

Let $S_r$ be the real magnetization of the tissue, to measure it the magnetization is flipped on the transverse plane. If the flip angle is $\frac{\pi}{2}$, then $S_r$ is projected onto transverse plane with equal magnitude initially, but during the measurement time (echo time, $T_E$), it is subjected to transverse relaxation. So, the measured magnetization is equal to this $T_2{}^*$ weighted value of $S_r$.

The first measurement was performed before the passage of the bolus. Let the measured magnetization be denoted as $S_{pre}$ and the transverse relaxation constant as $T_{2pre}{}^*$;

$$S_{pre} = S_r.e^{\frac{-T_E}{T^*_{2(pre)}}} \tag{A.1}$$

. The magnetization is also measured during the bolus passage and denoted as $S_{post}$

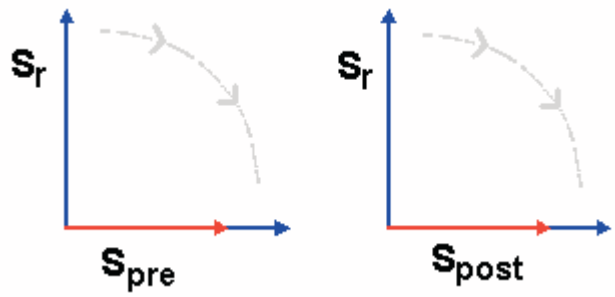


**Figure A.1** Before the bolus passage, the equilibrium magnetization is flipped on the transverse plane. During the sampling of k-space, transverse magnetization is subject to transverse relaxation, so transverse magnetization become $S_{pre}$ after a time interval $T_E$, which is also named as $T_2^*$-weighted equilibrium magnetization. Similiarly, the same procedure is applied during the passage of bolus to obtain $S_{post}$. The ratio of two magnetizations are concentration weighted.

where transverse relaxation constant as $T_{2post}{}^{*}$;

$$S_{post} = S_r.e^{\frac{-T_E}{T^*_{2(post)}}} \tag{A.2}$$

.

Combining the two equations [14] :

$$\begin{aligned} S_{post} &= S_{pre}.e^{\frac{T_E}{T^*_{2(pre)}}}.e^{\frac{-T_E}{T^*_{2(post)}}} \\ &= S_{pre}.e^{T_E.R^*_{2(pre)}}.e^{-T_E.R^*_{2(post)}} \\ &= S_{pre}.e^{-T_E.\Delta R^*_2} \end{aligned} \tag{A.3}$$

.

Now, it is assumed that the change in transverse relaxivity of the voxel is directly proportional to the concentration of the agent in the voxel [15] ;

$$\begin{aligned} \Delta R^*_2 &= \frac{4}{3}\pi\gamma\chi^m_{CA}B_0C_{VOI} \\ &= k.C_{VOI} \end{aligned} \tag{A.4}$$

where k is the calibration factor.

Then at any time t, the tracer concentration in the VOI can be calculated as:

$$C_{VOI}(t) = -\frac{1}{k.T_E}ln(\frac{S(t)}{S_{pre}}) \tag{A.5}$$

.

[14] $R_2$ is transverse relaxivity where $R^*_{2(pre)} = \frac{1}{T^*_{2(pre)}}$ and $R^*_{2(post)} = \frac{1}{T^*_{2(post)}}$.

[15] $\gamma$ is gyromagnetic ratio, $\chi^m_{CA}$ is molar susceptibility of the contrast agent, $B_0$ is the magnetic field in the absence of the sample.

# APPENDIX B. Information Content of Residue Function R(t)

Residue function R(t) is defined in Eq.4.10. $R(t_2\text{-}t_1)$ is the fraction of agent that entered the voxel at time $t_1$ and still in the voxel at time $t_2$.

R(t) is also related with h(t). The fraction of agent that leaves the voxel between t and t+dt is h(t), so it is also equal to the change in R(t);

$$\frac{dR}{dt} = -h(t) \tag{B.1}$$

.

MTT is calculated as Eq.4.6, in terms of h(t). Additionally,

$$\begin{aligned} MTT &= \int_0^\infty t.h(t) \\ &= \int_0^\infty t.dR \ \ (Integrating \ \ by \ \ parts \ \ yields) \\ &= t.R(t)|_0^\infty + \int_0^\infty R(t)dt \\ &= \int_0^\infty R(t)dt \end{aligned} \tag{B.2}$$

It is verified that, the integral of R(t) gives MTT.

As described before, CBF.$\triangle$t.R(t) is obtained as the result of deconvolution in DSC method. Knowing $\triangle$t is a scan parameter, one can easily obtain CBF, from the global maxima of CBF.$\triangle$t.R(t). Thus two perfusion parameters are directly obtained from the impulse response of the tissue.

However, to calculate CBV, one has to call central value theorem that states;

$$CBV = CBF \times MTT \tag{B.3}$$

for brain voxel. This is one of the ways of calculating CBV.

# APPENDIX C. General Kinetic Model

A general kinetic model is developed by Buxton et al.[44] to describe the measured change of magnetization difference in time, $\Delta$M(t). Under some assumption, the general model reduces to standard model given in Eq.7.3 and extensively used in ASL literature for quantification of CBF.

General model consists of three functions;

- c(t) is the normalized *delivery function*. It describes the arterial concentration of concentration arriving at the voxel at time t.
- r(t,t') is the *residue function*. It describes the fraction of tagged water molecules that arrived the imaging slice at time t' and still in the imaging slice at time t.
- m(t,t') is the *magnetization relaxation function*. It describes the fraction of the original longitudinal magnetization tag carried by the water molecules that arrived at time t' and remains in the imaging slice at time t.

Then, $\Delta$M(t) can be calculated as the weighted sum of magnetizations carried to the imaging slice by tagged water up to time t. These weights are the multiplication of residue and magnetization relaxation functions. Using these definitions one can write,

$$\begin{aligned} \Delta M(t) &= 2.M_{0B}.CBF.\int_0^t c(t')r(t-t')m(t-t')dt' \\ &= 2.M_{0B}.CBF.c(t) \otimes [r(t).m(t)] \end{aligned} \tag{C.1}$$

.

Any tracer kinetic experiment in PASL can be modeled using the defined parameters and Eq.C.1. Adjusting the behavior of three model parameters, one can construct any specific model.

Applying some assumptions on the behavior of model parameters results the reduction of general model into standard model. These assumptions are;

1. Tagged blood is carried to the imaging slice via uniform plug flow. c(t) is zero until t>$\delta$t, during the passage of the inverted bolus it is $e^{-t/T_{1B}}$ because it is subject to $T_1$ decay with the decay constant of blood, $T_{1B}$. After the trailing edge of the bolus passed the imaging slice, it becomes zero again.

2. First compartment kinetics is valid for the water exchange between the blood and tissue. It means that the concentration ratios of tagged blood in tissue and blood is equal to the steady state blood-brain partition coefficient $\lambda$ at every time. The amount of magnetized tag carried out is CBF.$M_V$.$\Delta$t=(CBF/$\lambda$).$M_T$.$\Delta$t where $M_V$ is the venous magnetization and $M_T$ is the tissue magnetization. With these assumptions r(t) = $e^{-ft/\lambda}$

3. As the tagged water reaches to the imaging slice it is completely extracted from the vascular space to the tissue compartment. Thus, it starts to relax with the $T_1$ of tissue immediately after it arrives to the imaging voxel, m(t)=$e^{-t/T_1}$

To summarize, parameters can be written as,

$$\begin{aligned} c(t) &= 0 && 0 < t < \delta t \\ &= e^{-t/T_{1B}} && \delta t < t < \tau + \delta t \\ &= 0 && \tau + \delta t < t \\ r(t) &= e^{-ft/\lambda} \\ m(t) &= e^{-t/T_1} \end{aligned} \tag{C.2}$$

for standard model.

When the parameters in Eq.C.2 is applied to Eq.C.2, Eq.7.3 is obtained in a formal way. The coefficient q can be calculated as;

$$\begin{aligned} q &= \frac{e^{kt}(e^{-kt}-e^{-kt})}{k(t-\delta t)} \qquad \delta t < t < \tau + \delta t \\ q &= \frac{e^{kt}(e^{-kt}-e^{-k(\tau+\delta t)})}{k\tau} \qquad \tau + \delta t < t \end{aligned} \tag{C.3}$$

where;

$$\begin{aligned} k &= \frac{1}{T_{1B}} - \frac{1}{T_{1'}} \\ \frac{1}{T_{1'}} &= \frac{1}{T_1} - \frac{f}{\lambda} \end{aligned} \tag{C.4}$$

# APPENDIX D. Determination of $M_{0B}$

It is necessary to determine the $T_2^*$ equilibrium magnetization of blood ($M_{0B}$) for the absolute quantification using ASL.

For that purpose, firstly the the $T_2^*$ equilibrium magnetization of white matter ($M_{0wm}$) must be found. This will be done by using the masks obtained in the segmentation and $M_0$ maps of the brain. WM mask is multiplied pixelwise with $M_0$ map, a slice which consists of only WM pixels is obtained (Figure D.1). In the second step, to determine the ($M_{0wm}$), three distinct methods can be used;

1. Finding the arithmetical mean of the non-zero elements in the masked image
2. Using the $M_0$ of a perfect WM pixel, which has $T_1$ closest to the ideal $T_1$ WM found in the segmentation analysis.
3. By fitting a gaussian to the histogram of non-zero elements in the masked image. The expected value of the gaussian is accepted as $M_{0wm}$.

After the $M_{0wm}$ is found, it will be used in the equation below.

$$M_{0B} = RM_{0wm}e^{(1/T_{2wm}-1/T_{2B})T_E} \tag{D.1}$$


**Figure D.1** Pixelwise multiplication of $M_0$ map with the white matter mask gives the slice with only $M_0$ of WM's.

In Eq. D.1, $T_{2wm}$, $T_{2B}$ are assumed values given in the literature [16] , $T_E$ is the scan parameter and R can be accepted as proposed by Wong et al [36]. In that work, R is measured as the ratio of proton density of blood in the sagittal sinus to that of white matter [17] , by using a proton density weighted, high resolution, gradient-echo conventional image (with $T_E$ = 5ms, $T_R$ = 1000ms, $\alpha = 10^o$). Using the determined parameters with Eq.D.1, $M_{0B}$ is calculated.

[16] $T_{2wm}$ & $T_{2B}$ is replaced by $T^*_{2wm}$ & $T^*_{2B}$ if gradient echo sequence is used instead of spin echo.
[17] R is measured as 1.06

# REFERENCES


1. Huntington's Outresearch Project For Education (HOPES) at Stanford, Brain Tutorial: 2003. Avalible: http://hopes.stanford.edu/basics/braintut/ab0.html.

2. Medical Illustration, Human Anatomy Drawing: 1999. Avalible: http://catalog.nucleusinc.com.

3. Meier, P., and K. L. Zierler, "On the theory of the indicator-dilution method for measurement of blood flow and volume.," *J Appl Physiol*, Vol. 6, pp. 731–744, Jun 1954.

4. Kety, S. S., and C. F. Schmidt, "The nitrous oxide method for the quantitative determination of cerebral blood flow in man: Theory, procedure and normal values," *J Clin Invest*, Vol. 27, pp. 476–483, Jul 1948.

5. Campus Medica, MRI Illustrastions: 2007. Avalible: http://www.e-mri.org.

6. Scott, M. L. J., *Towards a Quantitative Methodology for the Assessment of Cerebral Blood Flow in Magnetic Resonance Imaging*. PhD thesis, The University of Manchester, School of Medicine, 2005.

7. Perkiö, J., H. J. Aronen, A. Kangasmäki, Y. Liu, J. Karonen, S. Savolainen, and L. Østergaard, "Evaluation of four postprocessing methods for determination of cerebral blood volume and mean transit time by dynamic susceptibility contrast imaging.," *Magn Reson Med*, Vol. 47, pp. 973–981, May 2002.

8. Wolf, R. L., and J. A. Detre, "Clinical neuroimaging using arterial spin-labeled perfusion magnetic resonance imaging.," *Neurotherapeutics*, Vol. 4, pp. 346–359, Jul 2007.

9. Sidaros, K., *Slice Profile Effects in MR Perfusion Imaging Using Pulsed Arterrial Spin Labeling*. PhD thesis, Technical University of Denmark, 2002.

10. Luh, W. M., E. C. Wong, P. A. Bandettini, and J. S. Hyde, "Quipss ii with thin-slice ti1 periodic saturation: a method for improving accuracy of quantitative perfusion imaging using pulsed arterial spin labeling.," *Magn Reson Med*, Vol. 41, pp. 1246–1254, Jun 1999.

11. Figueiredo, P. M., S. Clare, and P. Jezzard, "Quantitative perfusion measurements using pulsed arterial spin labeling: effects of large region-of-interest analysis.," *J Magn Reson Imaging*, Vol. 21, pp. 676–682, Jun 2005.

12. Ganong, W. F., *Review of Medical Physiology*, McGraw-Hill, 22 ed., 2005.

13. Pocock, G., and C. Richards, *Human Physiology The Basis of Medicine*, Oxford University Press, 2 ed., 2004.

14. Sakoh, M., L. Røhl, C. Gyldensted, A. Gjedde, and L. Ostergaard, "Cerebral blood flow and blood volume measured by magnetic resonance imaging bolus tracking after acute stroke in pigs: comparison with [(15)o]h(2)o positron emission tomography.," *Stroke*, Vol. 31, pp. 1958–1964, Aug 2000.

15. Wintermark, M., M. Sesay, E. Barbier, K. Borbély, W. P. Dillon, J. D. Eastwood, T. C. Glenn, C. B. Grandin, S. Pedraza, J.-F. Soustiel, T. Nariai, G. Zaharchuk, J.-M. Caillé, V. Dousset, and H. Yonas, "Comparative overview of brain perfusion imaging techniques.," *Stroke*, Vol. 36, pp. e83–e99, Sep 2005.

16. Martin, C. C., P. A. Jerabek, L. D. Nickerson, and P. T. Fox, "Effect of partition coefficient, permeability surface product, and radioisotope on the signal-to-noise ratio in pet functional brain mapping: a computer simulation.," *Hum Brain Mapp*, Vol. 7, no. 3, pp. 151–160, 1999.

17. Raichle, M. E., W. R. Martin, P. Herscovitch, M. A. Mintun, and J. Markham, "Brain blood flow measured with intravenous h2(15)o. ii. implementation and validation.," *J Nucl Med*, Vol. 24, pp. 790–798, Sep 1983.

18. Donahue, M. J., H. Lu, C. K. Jones, J. J. Pekar, and P. C. M. van Zijl, "An account of the discrepancy between mri and pet cerebral blood flow measures. a high-field mri investigation.," *NMR Biomed*, Vol. 19, pp. 1043–1054, Dec 2006.

19. Griffiths, P. D., N. Hoggard, W. R. Dannels, and I. D. Wilkinson, "In vivo measurement of cerebral blood flow: a review of methods and applications.," *Vasc Med*, Vol. 6, no. 1, pp. 51–60, 2001.

20. Taber, K. H., K. J. Black, and R. A. Hurley, "Blood flow imaging of the brain: 50 years experience.," *J Neuropsychiatry Clin Neurosci*, Vol. 17, no. 4, pp. 441–446, 2005.

21. Wintermark, M., P. Maeder, J. P. Thiran, P. Schnyder, and R. Meuli, "Quantitative assessment of regional cerebral blood flows by perfusion ct studies at low injection rates: a critical review of the underlying theoretical models.," *Eur Radiol*, Vol. 11, no. 7, pp. 1220–1230, 2001.

22. Phillips, M. D., "Brain perfusion imaging," *Seminars in Cerebrovascular Diseases and Stroke*, Vol. 1, no. 4, 2001.

23. Wintermark, M., J. P. Thiran, P. Maeder, P. Schnyder, and R. Meuli, "Simultaneous measurement of regional cerebral blood flow by perfusion ct and stable xenon ct: a validation study.," *AJNR Am J Neuroradiol*, Vol. 22, pp. 905–914, May 2001.

24. Zierler, K. L., "Theoretical basis of indicator-dilution methods for measuring flow and volume," *Circ. Rrs*, Vol. 10, pp. 393–407, 1962.

25. Ostergaard, L., R. M. Weisskoff, D. A. Chesler, C. Gyldensted, and B. R. Rosen, "High resolution measurement of cerebral blood flow using intravascular tracer bolus passages. part i: Mathematical approach and statistical analysis.," *Magn Reson Med*, Vol. 36, pp. 715–725, Nov 1996.

26. Golay, X., E. T. Petersen, I. Zimine, and T. C. C. Lim, "Arterial spin labeling: a one-stop-shop for measurement of brain perfusion in the clinical settings.," *Conf Proc IEEE Eng Med Biol Soc*, Vol. 1, pp. 4320–4323, 2007.

27. Kety, S. S., and C. F. Schmidt, "The determinations of cerebral blood flow in man by the use of nitrous oxide in low concentrations," *Am. J. Physiol.*, Vol. 143, p. 53, 1945.

28. Liang Z., L. P. C., *Principles of Magnetic Resonance Imaging -A signal Processing Perspective-*, IEEE Series in Biomdical Engineering, 2000.

29. Buxton, R., *Introduction to Functional Magnetic Resonance Imaging*, Cambridge University Press, 2002.

30. Cohen, M., *Echo Planar Imaging and Functional MR*, 1998.

31. Barbier, E. L., L. Lamalle, and M. Décorps, "Methodology of brain perfusion imaging.," *J Magn Reson Imaging*, Vol. 13, pp. 496–520, Apr 2001.

32. Edelman, R. R., B. Siewert, D. G. Darby, V. Thangaraj, A. C. Nobre, M. M. Mesulam, and S. Warach, "Qualitative mapping of cerebral blood flow and functional localization with echo-planar mr imaging and signal targeting with alternating radio frequency.," *Radiology*, Vol. 192, pp. 513–520, Aug 1994.

33. Wong, E. C., R. B. Buxton, and L. R. Frank, "Implementation of quantitative perfusion imaging techniques for functional brain mapping using pulsed arterial spin labeling.," *NMR Biomed*, Vol. 10, no. 4-5, pp. 237–249, 1997.

34. Wong, E. C., "Quantifying cbf with pulsed asl: technical and pulse sequence factors.," *J Magn Reson Imaging*, Vol. 22, pp. 727–731, Dec 2005.

35. Kim, S. G., "Quantification of relative cerebral blood flow change by flow-sensitive alternating inversion recovery (fair) technique: application to functional mapping.," *Magn Reson Med*, Vol. 34, pp. 293–301, Sep 1995.

36. Wong, E. C., R. B. Buxton, and L. R. Frank, "Quantitative imaging of perfusion using a single subtraction (quipss and quipss ii).," *Magn Reson Med*, Vol. 39, pp. 702–708, May 1998.

37. Noguchi, T., T. Yoshiura, A. Hiwatashi, O. Togao, K. Yamashita, K. Kobayashi, F. Mihara, and H. Honda, "Quantitative perfusion imaging with pulsed arterial spin labeling: a phantom study.," *Magn Reson Med Sci*, Vol. 6, no. 2, pp. 91–97, 2007.

38. Wang, J., D. C. Alsop, L. Li, J. Listerud, J. B. Gonzalez-At, M. D. Schnall, and J. A. Detre, "Comparison of quantitative perfusion imaging using arterial spin labeling at 1.5 and 4.0 tesla.," *Magn Reson Med*, Vol. 48, pp. 242–254, Aug 2002.

39. Wang, J., D. J. Licht, G.-H. Jahng, C.-S. Liu, J. T. Rubin, J. Haselgrove, R. A. Zimmerman, and J. A. Detre, "Pediatric perfusion imaging using pulsed arterial spin labeling.," *J Magn Reson Imaging*, Vol. 18, pp. 404–413, Oct 2003.

40. Stanisz, G. J., E. E. Odrobina, J. Pun, M. Escaravage, S. J. Graham, M. J. Bronskill, and R. M. Henkelman, "T1, t2 relaxation and magnetization transfer in tissue at 3t.," *Magn Reson Med*, Vol. 54, pp. 507–512, Sep 2005.

41. Warmuth, C., M. Gunther, and C. Zimmer, "Quantification of blood flow in brain tumors: comparison of arterial spin labeling and dynamic susceptibility-weighted contrast-enhanced mr imaging.," *Radiology*, Vol. 228, pp. 523–532, Aug 2003.

42. Campbell, A. M., and C. Beaulieu, "Pulsed arterial spin labeling parameter optimization for an elderly population.," *J Magn Reson Imaging*, Vol. 23, pp. 398–403, Mar 2006.

43. Luh W.M, Donahue K., H. J., "Estimating of t1 relaxation times and fractional volumes of brain tissues using using epi-based t1 maps," in *ISMRM Prooceding*, ISMRM, 1999.

44. Buxton, R. B., L. R. Frank, E. C. Wong, B. Siewert, S. Warach, and R. R. Edelman, "A general kinetic model for quantitative perfusion imaging with arterial spin labeling.," *Magn Reson Med*, Vol. 40, pp. 383–396, Sep 1998.

45. Bolar D.S, T. Benner, R. H. M. P. C. W. D. G. P. W. A. S., "Perfusion imaging of hemangioblastoma: Implications for using arterial spin labeling to characterize tumor hemodynamics," in *ISMRM Prooceding*, ISMRM, 2005.

46. Xie J., Gallichan D., G. R. J. P., "Optimal design of pulsed asl sampling schedules," in *ISMRM Prooceding*, ISMRM, 2007.

47. Frackowiak, R. S., G. L. Lenzi, T. Jones, and J. D. Heather, "Quantitative measurement of regional cerebral blood flow and oxygen metabolism in man using 15o and positron emission tomography: theory, procedure, and normal values.," *J Comput Assist Tomogr*, Vol. 4, pp. 727–736, Dec 1980.

48. Leenders, K. L., D. Perani, A. A. Lammertsma, J. D. Heather, P. Buckingham, M. J. Healy, J. M. Gibbs, R. J. Wise, J. Hatazawa, and S. Herold, "Cerebral blood flow, blood volume and oxygen utilization. normal values and effect of age.," *Brain*, Vol. 113 ( Pt 1), pp. 27–47, Feb 1990.

49. Rempp, K. A., G. Brix, F. Wenz, C. R. Becker, F. Gückel, and W. J. Lorenz, "Quantification of regional cerebral blood flow and volume with dynamic susceptibility contrast-enhanced mr imaging.," *Radiology*, Vol. 193, pp. 637–641, Dec 1994.

50. Wansapura, J. P., S. K. Holland, R. S. Dunn, and W. S. Ball, "Nmr relaxation times in the human brain at 3.0 tesla.," *J Magn Reson Imaging*, Vol. 9, pp. 531–538, Apr 1999.

51. Benner, T., S. Heiland, G. Erb, M. Forsting, and K. Sartor, "Accuracy of gamma-variate fits to concentration-time curves from dynamic susceptibility-contrast enhanced mri: influence of time resolution, maximal signal drop and signal-to-noise.," *Magn Reson Imaging*, Vol. 15, no. 3, pp. 307–317, 1997.

52. Calamante, F., D. G. Gadian, and A. Connelly, "Quantification of perfusion using bolus tracking magnetic resonance imaging in stroke: assumptions, limitations, and potential implications for clinical use.," *Stroke*, Vol. 33, pp. 1146–1151, Apr 2002.

53. Cha, S., E. A. Knopp, G. Johnson, S. G. Wetzel, A. W. Litt, and D. Zagzag, "Intracranial mass lesions: dynamic contrast-enhanced susceptibility-weighted echo-planar perfusion mr imaging.," *Radiology*, Vol. 223, pp. 11–29, Apr 2002.

54. Cha, S., S. Lu, G. Johnson, and E. A. Knopp, "Dynamic susceptibility contrast mr imaging: correlation of signal intensity changes with cerebral blood volume measurements.," *J Magn Reson Imaging*, Vol. 11, pp. 114–119, Feb 2000.

55. Jackson, A., "Analysis of dynamic contrast enhanced mri.," *Br J Radiol*, Vol. 77 Spec No 2, pp. S154–S166, 2004.

56. Kiselev, V. G., "On the theoretical basis of perfusion measurements by dynamic susceptibility contrast mri.," *Magn Reson Med*, Vol. 46, pp. 1113–1122, Dec 2001.

57. Murase, K., M. Shinohara, and Y. Yamazaki, "Accuracy of deconvolution analysis based on singular value decomposition for quantification of cerebral blood flow using dynamic susceptibility contrast-enhanced magnetic resonance imaging.," *Phys Med Biol*, Vol. 46, pp. 3147–3159, Dec 2001.

58. Ostergaard, L. O., "New developments in perfusion imaging by bolus tracking.," *J Neuroradiol*, Vol. 32, pp. 315–320, Dec 2005.

59. Clare, S., and P. Jezzard, "Rapid t(1) mapping using multislice echo planar imaging.," *Magn Reson Med*, Vol. 45, pp. 630–634, Apr 2001.

60. Gowland, P., and P. Mansfield, "Accurate measurement of t1 in vivo in less than 3 seconds using echo-planar imaging.," *Magn Reson Med*, Vol. 30, pp. 351–354, Sep 1993.

61. Jones, C. K., *T2 Decay Curve Acquisition and Analysis in MRI Noise Considerations, Short T2, and B1 Field Encoding.* PhD thesis, THE UNIVERSITY OF BRITISH COLUMBIA, 2003.

62. Kim, S. G., X. Hu, and K. Ugurbil, "Accurate t1 determination from inversion recovery images: application to human brain at 4 tesla.," *Magn Reson Med*, Vol. 31, pp. 445–449, Apr 1994.

63. Alsop, D. C., and J. A. Detre, "Multisection cerebral blood flow mr imaging with continuous arterial spin labeling.," *Radiology*, Vol. 208, pp. 410–416, Aug 1998.

64. Alsop, D. C., and J. A. Detre, "Reduced transit-time sensitivity in noninvasive magnetic resonance imaging of human cerebral blood flow.," *J Cereb Blood Flow Metab*, Vol. 16, pp. 1236–1249, Nov 1996.

65. Alsop, D. C., J. A. Detre, and M. Grossman, "Assessment of cerebral blood flow in alzheimer's disease by spin-labeled magnetic resonance imaging.," *Ann Neurol*, Vol. 47, pp. 93–100, Jan 2000.

66. Arbab, A. S., S. Aoki, K. Toyama, N. Miyazawa, H. Kumagai, T. Umeda, T. Arai, T. Araki, H. Kabasawa, and Y. Takahashi, "Quantitative measurement of regional cerebral blood flow with flow-sensitive alternating inversion recovery imaging: comparison with [iodine 123]-iodoamphetamin single photon emission ct.," *AJNR Am J Neuroradiol*, Vol. 23, pp. 381–388, Mar 2002.

67. Barbier, E. L., A. C. Silva, H. J. Kim, D. S. Williams, and A. P. Koretsky, "Perfusion analysis using dynamic arterial spin labeling (dasl).," *Magn Reson Med*, Vol. 41, pp. 299–308, Feb 1999.

68. Boss, A., P. Martirosian, C. D. Claussen, and F. Schick, "Quantitative asl muscle perfusion imaging using a fair-truefisp technique at 3.0 t.," *NMR Biomed*, Vol. 19, pp. 125–132, Feb 2006.

69. Brown, G. G., C. Clark, and T. T. Liu, "Measurement of cerebral perfusion with arterial spin labeling: Part 2. applications.," *J Int Neuropsychol Soc*, Vol. 13, pp. 526–538, May 2007.

70. Calamante, F., S. R. Williams, N. van Bruggen, K. K. Kwong, and R. Turner, "A model for quantification of perfusion in pulsed labelling techniques.," *NMR Biomed*, Vol. 9, pp. 79–83, Apr 1996.

71. Campbell, A. M., and C. Beaulieu, "Comparison of multislice and single-slice acquisitions for pulsed arterial spin labeling measurements of cerebral perfusion.," *Magn Reson Imaging*, Vol. 24, pp. 869–876, Sep 2006.

72. Zhang, W., D. S. Williams, and A. P. Koretsky, "Measurement of rat brain perfusion by nmr using spin labeling of arterial water: in vivo determination of the degree of spin labeling.," *Magn Reson Med*, Vol. 29, pp. 416–421, Mar 1993.

73. Zhang, W., A. C. Silva, D. S. Williams, and A. P. Koretsky, "Nmr measurement of perfusion using arterial spin labeling without saturation of macromolecular spins.," *Magn Reson Med*, Vol. 33, pp. 370–376, Mar 1995.

74. Zhang, Y., H. K. Song, J. Wang, A. Techawiboonwong, and F. W. Wehrli, "Spatially-confined arterial spin-labeling with fair.," *J Magn Reson Imaging*, Vol. 22, pp. 119–124, Jul 2005.

75. Zhou, J., and P. C. van Zijl, "Effect of transit times on quantification of cerebral blood flow by the fair t(1)-difference approach.," *Magn Reson Med*, Vol. 42, pp. 890–894, Nov 1999.

76. Axel, L., "Cerebral blood flow determination by rapid-sequence computed tomography: theoretical analysis.," *Radiology*, Vol. 137, pp. 679–686, Dec 1980.

77. Wang, J., G. K. Aguirre, D. Y. Kimberg, A. C. Roc, L. Li, and J. A. Detre, "Arterial spin labeling perfusion fmri with very low task frequency.," *Magn Reson Med*, Vol. 49, pp. 796–802, May 2003.

78. Wang, J., D. C. Alsop, H. K. Song, J. A. Maldjian, K. Tang, A. E. Salvucci, and J. A. Detre, "Arterial transit time imaging with flow encoding arterial spin tagging (feast).," *Magn Reson Med*, Vol. 50, pp. 599–607, Sep 2003.

79. Wang, J., L. Li, A. C. Roc, D. C. Alsop, K. Tang, N. S. Butler, M. D. Schnall, and J. A. Detre, "Reduced susceptibility effects in perfusion fmri with single-shot spin-echo epi acquisitions at 1.5 tesla.," *Magn Reson Imaging*, Vol. 22, pp. 1–7, Jan 2004.

80. Wang, J., and D. J. Licht, "Pediatric perfusion mr imaging using arterial spin labeling.," *Neuroimaging Clin N Am*, Vol. 16, pp. 149–67, ix, Feb 2006.

81. Williams, D. S., J. A. Detre, J. S. Leigh, and A. P. Koretsky, "Magnetic resonance imaging of perfusion using spin inversion of arterial water.," *Proc Natl Acad Sci U S A*, Vol. 89, pp. 212–216, Jan 1992.

82. Wong, E. C., M. Cronin, W.-C. Wu, B. Inglis, L. R. Frank, and T. T. Liu, "Velocity-selective arterial spin labeling.," *Magn Reson Med*, Vol. 55, pp. 1334–1341, Jun 2006.

83. Wong, E. C., W. M. Luh, and T. T. Liu, "Turbo asl: arterial spin labeling with higher snr and temporal resolution.," *Magn Reson Med*, Vol. 44, pp. 511–515, Oct 2000.

84. Yang, Y., J. A. Frank, L. Hou, F. Q. Ye, A. C. McLaughlin, and J. H. Duyn, "Multislice imaging of quantitative cerebral perfusion with pulsed arterial spin labeling.," *Magn Reson Med*, Vol. 39, pp. 825–832, May 1998.

85. Ye, F. Q., V. S. Mattay, P. Jezzard, J. A. Frank, D. R. Weinberger, and A. C. McLaughlin, "Correction for vascular artifacts in cerebral blood flow values measured by using arterial spin tagging techniques.," *Magn Reson Med*, Vol. 37, pp. 226–235, Feb 1997.

86. Thomas, D. L., "Arterial spin labeling in small animals: methods and applications to experimental cerebral ischemia.," *J Magn Reson Imaging*, Vol. 22, pp. 741–744, Dec 2005.

87. Thomas, D. L., M. F. Lythgoe, D. G. Gadian, and R. J. Ordidge, "In vivo measurement of the longitudinal relaxation time of arterial blood (t1a) in the mouse using a pulsed arterial spin labeling approach.," *Magn Reson Med*, Vol. 55, pp. 943–947, Apr 2006.

88. Sugahara, H., "Brain blood perfusion hypothesis for migraine, anger, and epileptic attacks.," *Med Hypotheses*, Vol. 62, no. 5, pp. 766–769, 2004.

89. Silva, A. C., W. Zhang, D. S. Williams, and A. P. Koretsky, "Estimation of water extraction fractions in rat brain using magnetic resonance measurement of perfusion with arterial spin labeling.," *Magn Reson Med*, Vol. 37, pp. 58–68, Jan 1997.

90. Silva, A. C., S. G. Kim, and M. Garwood, "Imaging blood flow in brain tumors using arterial spin labeling.," *Magn Reson Med*, Vol. 44, pp. 169–173, Aug 2000.

91. Silva, A. C., D. S. Williams, and A. P. Koretsky, "Evidence for the exchange of arterial spin-labeled water with tissue water in rat brain from diffusion-sensitized measurements of perfusion.," *Magn Reson Med*, Vol. 38, pp. 232–237, Aug 1997.

92. Silva, A. C., "Perfusion-based fmri: insights from animal models.," *J Magn Reson Imaging*, Vol. 22, pp. 745–750, Dec 2005.

93. Reishofer, G., F. Fazekas, S. Keeling, C. Enzinger, F. Payer, J. Simbrunner, and R. Stollberger, "Minimizing macrovessel signal in cerebral perfusion imaging using independent component analysis.," *Magn Reson Med*, Vol. 57, pp. 278–288, Feb 2007.

94. Petersen, E. T., T. Lim, and X. Golay, "Model-free arterial spin labeling quantification approach for perfusion mri.," *Magn Reson Med*, Vol. 55, pp. 219–232, Feb 2006.

95. Parkes, L. M., and P. S. Tofts, "Improved accuracy of human cerebral blood perfusion measurements using arterial spin labeling: accounting for capillary water permeability.," *Magn Reson Med*, Vol. 48, pp. 27–41, Jul 2002.

96. Paiva, F. F., A. Tannús, and A. C. Silva, "Measurement of cerebral perfusion territories using arterial spin labelling.," *NMR Biomed*, Vol. 20, pp. 633–642, Nov 2007.

97. Detre, J. A., D. C. Alsop, L. R. Vives, L. Maccotta, J. W. Teener, and E. C. Raps, "Noninvasive mri evaluation of cerebral blood flow in cerebrovascular disease.," *Neurology*, Vol. 50, pp. 633–641, Mar 1998.

98. Detre, J. A., J. S. Leigh, D. S. Williams, and A. P. Koretsky, "Perfusion imaging.," *Magn Reson Med*, Vol. 23, pp. 37–45, Jan 1992.

99. Duyn, J. H., P. van Gelderen, L. Talagala, A. Koretsky, and J. A. de Zwart, "Technological advances in mri measurement of brain perfusion.," *J Magn Reson Imaging*, Vol. 22, pp. 751–753, Dec 2005.

100. Eastwood, J. D., C. A. Holder, P. A. Hudgins, and A. W. Song, "Magnetic resonance imaging with lateralized arterial spin labeling.," *Magn Reson Imaging*, Vol. 20, pp. 583–586, Oct 2002.

101. Edelman, R. R., and Q. Chen, "Epistar mri: multislice mapping of cerebral blood flow.," *Magn Reson Med*, Vol. 40, pp. 800–805, Dec 1998.

102. Ewing, J. R., Y. Cao, R. A. Knight, and J. D. Fenstermacher, "Arterial spin labeling: validity testing and comparison studies.," *J Magn Reson Imaging*, Vol. 22, pp. 737–740, Dec 2005.

103. Günther, M., M. Bock, and L. R. Schad, "Arterial spin labeling in combination with a look-locker sampling strategy: inflow turbo-sampling epi-fair (its-fair).," *Magn Reson Med*, Vol. 46, pp. 974–984, Nov 2001.

104. Günther, M., K. Oshio, and D. A. Feinberg, "Single-shot 3d imaging techniques improve arterial spin labeling perfusion measurements.," *Magn Reson Med*, Vol. 54, pp. 491–498, Aug 2005.

105. Hendrikse, J., J. van der Grond, H. Lu, P. C. M. van Zijl, and X. Golay, "Flow territory mapping of the cerebral arteries with regional perfusion mri.," *Stroke*, Vol. 35, pp. 882–887, Apr 2004.

106. Koziak, A. M., J. Winter, T.-Y. Lee, R. T. Thompson, and K. S. S. Lawrence, "Validation study of a pulsed arterial spin labeling technique by comparison to perfusion computed tomography.," *Magn Reson Imaging*, Dec 2007.

107. van Laar, P. J., J. Hendrikse, X. Golay, H. Lu, M. J. P. van Osch, and J. van der Grond, "In vivo flow territory mapping of major brain feeding arteries.," *Neuroimage*, Vol. 29, pp. 136–144, Jan 2006.

108. Lawrence, K. S. S., J. A. Frank, and A. C. McLaughlin, "Effect of restricted water exchange on cerebral blood flow values calculated with arterial spin tagging: a theoretical investigation.," *Magn Reson Med*, Vol. 44, pp. 440–449, Sep 2000.

109. Liu, T. T., and G. G. Brown, "Measurement of cerebral perfusion with arterial spin labeling: Part 1. methods.," *J Int Neuropsychol Soc*, Vol. 13, pp. 517–525, May 2007.

110. Miranda, M. J., K. Olofsson, and K. Sidaros, "Noninvasive measurements of regional cerebral perfusion in preterm and term neonates by magnetic resonance arterial spin labeling.," *Pediatr Res*, Vol. 60, pp. 359–363, Sep 2006.

111. Nöth, U., G. E. Meadows, F. Kotajima, R. Deichmann, D. R. Corfield, and R. Turner, "Cerebral vascular response to hypercapnia: determination with perfusion mri at 1.5 and 3.0 tesla using a pulsed arterial spin labeling technique.," *J Magn Reson Imaging*, Vol. 24, pp. 1229–1235, Dec 2006.